Economic Geology
Vol. 93, 1998, pp. 981–1012

Geochemical and Geochronological Constraints on the Genesis of Au-Te Deposits at Cripple Creek, Colorado

KAREN D. KELLEY,[†]

U.S. Geological Survey, Denver Federal Center, Box 25046, Mail Stop 964, Denver, Colorado 80225

SAMUEL B. ROMBERGER,

Department of Geology and Geological Engineering, Colorado School of Mines, Golden, Colorado 80401

DAVID W. BEATY,

Chevron Petroleum Technology Company, P.O. Box 446, La Habra, California 90633

JEFFREY A. PONTIUS,

Independence Mining Company, Inc., 1053 Idaho Street, Elko, Nevada 89801

LAWRENCE W. SNEE,

U.S. Geological Survey, Denver Federal Center, Box 25046, Mail Stop 913, Denver, Colorado 80225

HOLLY J. STEIN,

Department of Earth Resources, Colorado State University, Fort Collins, Colorado 80523

AND TOMMY B. THOMPSON

Department of Geological Sciences, University of Nevada, Reno, Nevada 89557

Abstract

The Cripple Creek district (653 metric tons (t) of Au) consists of Au-Te veins and disseminated gold deposits that are spatially related to alkaline igneous rocks in an Oligocene intrusive complex. Vein paragenesis includes quartz-biotite-K feldspar-fluorite-pyrite followed by base metal sulfides and telluride minerals. Disseminated deposits consist of microcrystalline native gold with pyrite that are associated with zones of pervasive adularia.

New $^{40}Ar/^{39}Ar$ dates indicate that there was a complex magmatic and hydrothermal history. Relatively felsic rocks (tephriphonolite, trachyandesite, and phonolite) were emplaced into the complex over about 1 m.y., from 32.5 ± 0.1 (1σ) to 31.5 ± 0.1 Ma. A younger episode of phonolite emplacement outside of the complex is indicated by an age of 30.9 ± 0.1 Ma. Field relationships suggest that at least one episode of mafic and ultramafic dike emplacement occurred after relatively more felsic rocks and prior to the main gold mineralizing event. Only a single whole-rock date for mafic phonolite (which indicated a maximum age of 28.7 Ma) was obtained. However, constraints on the timing of mineralization are provided by paragenetically early vein minerals and K feldspar from the disseminated gold pyrite deposits. Early vein minerals (31.3 ± 0.1–29.6 ± 0.1 Ma) and K feldspar (29.8 ± 0.1 Ma) from the Cresson disseminated deposit, together with potassically altered phonolite adjacent to the Pharmacist vein (28.8 and 28.2 ± 0.1 Ma), suggest there was a protracted history of hydrothermal activity that began during the waning stages of phonolite and early mafic-ultramafic activity and continued, perhaps intermittently, for at least 2 m.y.

Estimated whole-rock $\delta^{18}O$ values of the alkaline igneous rocks range from 6.4 to 8.2 per mil. K feldspar and albite separates from igneous rocks have lead isotope compositions of $^{206}Pb/^{204}Pb$ = 17.90 to 18.10, $^{207}Pb/^{204}Pb$ = 15.51 to 15.53, and $^{208}Pb/^{204}Pb$ = 38.35 to 38.56. These isotopic compositions, together with major and trace element data, indicate that the phonolitic magmas probably evolved by fractional crystallization of an alkali basalt that assimilated lower crustal material. Upper crustal contamination of the magmas was not significant. The $^{206}Pb/^{204}Pb$ compositions of vein galenas almost entirely overlap those of phonolites, suggesting a genetic relationship between alkaline magmatism and mineralization. However, a trend toward higher $^{207}Pb/^{204}Pb$ (15.57–15.60) and $^{208}Pb/^{204}Pb$ ratios (38.94–39.48) of some galenas suggests a contribution to the ore fluid from surrounding Early Proterozoic rocks, probably through leaching by mineralizing fluids. Limited stable isotope compositions of quartz, K feldspar, and biotite from this and previous studies support a largely magmatic origin for the early vein fluids.

It is suggested that three features were collectively responsible for generating alkaline magmas and associated mineral deposits: (1) the timing of magmatism and mineralization, which coincided with the transition

[†] Corresponding author: email, kdkelley@usgs.gov

between subduction-related compression and extension related to continental rifting; (2) the location of Cripple Creek at the junction of four major Precambrian units and at the intersection of major northeast-trending regional structures with northwest-trending faults, which served as conduits for magmas and subsequent hydrothermal fluids; and (3) the complex magmatic history which included emplacement of relatively felsic magmas followed by successively more mafic magmas with time.

Introduction

LATE Mesozoic and Tertiary alkalic-related gold or gold-telluride vein and breccia deposits are located throughout the Rocky Mountain region from Canada to Mexico (Mutschler et al., 1985; Mutschler and Mooney, 1995). Cripple Creek is the largest of the Rocky Mountain gold-telluride districts. Since its discovery in 1891, the district has produced more than 653 metric tons (t) of Au (21 Moz), principally from narrow sheeted vein systems or from open-space fillings within mafic breccia bodies. The spectacular production history makes Cripple Creek one of the largest Au producers in the United States and one of the largest gold-telluride districts in the world.

The ore deposits of the district are localized within and adjacent to an elliptical northwest-trending diatreme complex that covers about 18 km^2 (Fig. 1). Most of the deposits are spatially associated with Tertiary breccias and alkaline igneous rocks that range in composition from phonolite to mafic and ultramafic silica-undersaturated rocks. Past gold production was primarily from high-grade gold-telluride vein deposits. However, exploration since 1989 has delineated previously undocumented low-grade, near-surface disseminated gold deposits that occur as broad zones in permeable rocks adjacent to major structures (Harris et al., 1993; Pontius, 1996). A proven and probable reserve of over 104 t of gold (3.7 Moz) with an additional drill-indicated resource of nearly 60 t (2.1 Moz) have been added to the district resource as a result of this exploration. Most of this mineralized rock is contained within the Cresson deposit. The Cresson open-pit mine is located in the south-central part of the district and is being operated by the Cripple Creek and Victor Gold Mining Company, which is a joint venture between Pikes Peak Mining Company and Golden Cycle Gold Corporation.

During the most productive mining years, which began in 1893, several comprehensive studies of the Cripple Creek district were conducted. The earliest (Cross and Penrose, 1895) included a geologic map with descriptions of the ore deposits and major types of intrusive rocks. Most mines in operation during their work at Cripple Creek had only reached depths of 30 to 60 m. Following the early work by Cross and Penrose (1895), rapid development of the mines necessitated new studies. In the most productive part of the district, over 20 shafts more than 300 m deep had been developed by the early 1900s. Comprehensive studies were undertaken that included detailed mapping of many of the 337 mines in the district and thorough descriptions of the mineralogy, texture, and field characteristics of the ores and host rocks (Lindgren and Ransome, 1906).

In the 1920s, studies were conducted to examine the downward persistence of the ore deposits (Loughlin and Koschmann, 1935). New geologic developments, most importantly the recognition of the Cresson "blowout," were described. The structural control of the gold deposits was also examined (Koschmann, 1949).

By 1962 the last underground mine and mill in the district were closed, although limited underground mining in the Ajax mine occurred between 1976 and 1986. Geochemical studies were initiated to locate low-grade gold that could be mined from the surface. The linear northwest-trending shape of the largest geochemical anomaly (Gott et al., 1969) supported the earlier conclusion that the distribution of gold deposits was controlled by a deep-rooted northwest-trending fissure zone. Aeromagnetic and gravity studies (Kleinkopf et al., 1970) further supported this conclusion, because geophysical anomalies could be correlated with the degree of alteration, which was most intense along the northwest-trending zone. Remote sensing studies (Taranik, 1990; Livo, 1994) further characterize the alteration and distribution of supergene iron oxides.

Over the past 20 yr, many studies have focused on the geology, mineralogy, alteration, and fluid inclusion characteristics of the deposits (Lane, 1976; Dwelley, 1984; Trippel, 1985; Saunders, 1986; Nelson, 1989; Wood, 1990; Seibel,

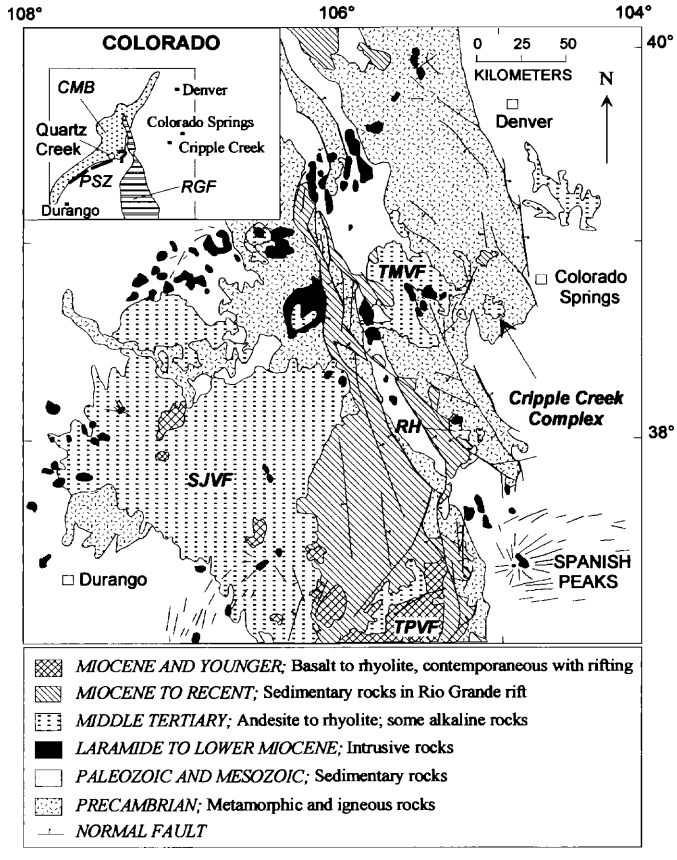

FIG 1. Major geologic features of central Colorado (after Lipman, 1981). RH = Rosita Hills volcanic center, SJVF = San Juan volcanic field, TMVF = Thirtynine Mile volcanic field, TPVF = Taos Plateau volcanic field. Inset: CMB = Colorado mineral belt, PSZ = Precambrian shear zone, RGF = Rio Grande rift (from Tweto and Sims, 1963).

1991; Burnett, 1995), as well as the petrographic and geochemical characteristics of the igneous rocks (Birmingham, 1987; Eriksson, 1987). Overview articles that summarize results from these studies include Thompson et al. (1985), Thompson (1989, 1992), and Pontius (1996).

The close spatial association between the deposits and alkaline igneous rocks have led many workers to suggest that the ore fluids were magmatically derived (Lindgren and Ransome, 1906; Thompson et al., 1985; Pontius, 1996). To place further constraints on the genesis of the deposits at Cripple Creek, we examined the temporal and genetic relationships between alkaline magmatism and gold mineralization using $^{40}Ar/^{39}Ar$ geochronology, major and trace element geochemistry, and stable and radiogenic isotope data.

Regional Geologic Setting

The Cripple Creek area lies in the southern Rocky Mountains in central Colorado (Fig. 1). The oldest rocks are high- to medium-grade schists and gneisses that were formed during Early Proterozoic time (1.8 Ga) when a series of volcanic- and back-arc complexes were accreted to the southern margin of the Archean craton (Reed et al., 1987). Three composite batholiths were intruded at about 1.7, 1.4, and 1.0 Ga. Deformation zones formed during the Proterozoic trend from north to northeast (Tweto, 1968, 1980).

Paleozoic sedimentary rocks record a long period of sedimentation followed by orogenic uplift and erosion during Late Paleozoic time (about 280–320 Ma). Mesozoic sedimentary rocks reflect nonmarine to marine sedimentation as orogenic activity waned and inland seas episodically invaded the area (Wallace, 1990). During Late Cretaceous to Tertiary time (about 70–40 Ma), northeast-directed regional compression related to the Laramide orogeny formed northwest-trending basement-cored uplifts and flanking basins throughout the Rocky Mountains. Igneous activity related to the Laramide orogeny included emplacement of alkaline to calcalkaline batholiths, stocks, sills, and dikes that were largely restricted to the broad northeast-trending Colorado mineral belt (Tweto and Sims, 1963; Fig. 1). The Laramide Rocky Mountains and their associated igneous rocks are the easternmost manifestations of the Laramide orogenic system.

The region experienced a tectonic quiescence from about 55 to 40 Ma that has been attributed to a temporary flattening of the subducted slab to such a low angle that igneous activity ceased (Lipman, 1981). Degradation of the mountainous terrane produced a widespread gentle erosion surface, termed the late Eocene erosion surface (Epis and Chapin, 1975), or Rocky Mountain surface (Evanoff and Chapin, 1994).

At about 40 to 35 Ma, there was a renewal of igneous activity in Colorado, manifested by the formation of the San Juan and Thirtynine Mile volcanic fields (Fig. 1). This renewal is attributed to increasing dips of the subduction system due to a decreased rate of plate convergence (Coney, 1972; Christiansen et al., 1992). Beginning in mid-Oligocene time, the tectonic regime in the southern Rocky Mountains gradually changed from compression to extension (Lipman, 1981). The major structural manifestation of extension in Colorado is the Rio Grande rift, a series of en echelon grabens and horsts that bisects New Mexico and continues into southern Colorado (Fig. 1). Large-scale uplift and north-northwest-trending block faulting in the southern Rocky Mountains occurred during rift development. Chapin and Seager (1975) and Chapin (1979) assign the onset of extension related to the Rio Grande rift zone to as early as 29 to 32 Ma in central New Mexico. The timing of the inception of extension in the northern segment of the rift (in Colorado) remains controversial. Lipman et al. (1978) first suggested that the northern segment of the rift began developing at about 27 Ma. However, some silicic alkaline volcanic and intrusive rocks, thought to represent an initial phase in the regional change to extensional tectonics in the southern Rocky Mountains, apparently were emplaced as early as 30 Ma in central Colorado (Lipman, 1981). In addition, Climax-type molybdenum deposits, associated with granitic rocks that are interpreted as having been emplaced during the extensional regime along the intersection of north-south-trending faults with earlier northeast-trending Laramide structures (Bookstrom, 1981), were formed at about 30 Ma. The thermal events associated with the formation of intrusions and large molybdenum deposits at Climax occurred between about 33 and 24 Ma (Cunningham et al., 1994; Wallace, 1995). Corresponding activity at Red Mountain (Urad and Henderson) spanned from about 30 to 27 Ma (Geissman et al., 1992). Alkaline rocks from Cripple Creek have ages similar to these Mo-bearing intrusions.

District Geology

The Cripple Creek district is localized within an elongated diatreme complex that covers about 18 km^2 (Fig. 2). The complex is a slightly elongate basin that trends northwest-southeast. The complex is localized at the junction between Proterozoic metamorphic rocks and three Proterozoic igneous intrusions. The earliest Proterozoic rocks are exposed along the northwest side of the complex beneath the town of Cripple Creek and include 1.8 Ga biotite-muscovite schists and gneisses (Xgs; Fig. 2). These rocks were first intruded by granodiorite (Xgd; Fig. 2) at 1.7 Ga (Wobus et al., 1976; Birmingham, 1987), followed by intrusion of the Cripple Creek Quartz Monzonite (Ycc; Fig. 2) at 1.43 Ga (Hutchinson and Hedge, 1968). The Pikes Peak Granite (Ypp; Fig. 2), dated at 1.04 Ga (Hedge, 1970), was the last Proterozoic intrusion.

The dominant rock unit within the complex is the Cripple Creek breccia (Thompson et al., 1985; Tbr, Fig. 2), which is heterolithic and ranges from diatremal breccias to poorly sorted airfall tuffs to bedded waterlain, volcaniclastic sedimentary units (Loughlin and Koschmann, 1935). The breccia clasts are angular to subangular fragments of Proterozoic metamorphic and igneous rocks, and Tertiary volcanic and sedimentary rocks, whereas matrix material consists of quartz, microcline, and rock fragments that are 0.5 to 2.0 mm in diameter (Thompson et al, 1985). Breccia textures include angular clast-supported breccias to those composed entirely of matrix-sized material (Seibel, 1991).

The Cripple Creek breccia and sedimentary rocks are found primarily within the complex (Fig. 2). Locally within the complex, the breccia is distinctly bedded (Loughlin and Koschmann, 1935). Carbonized tree trunks and local coaly layers occur in the breccia at depths as great as 300 m (Lindgren and Ransome, 1906). In the eastern and northern parts of the complex, the breccia is interbedded with lacustrine and fluvial sedimentary rocks. Locally, the lacustrine

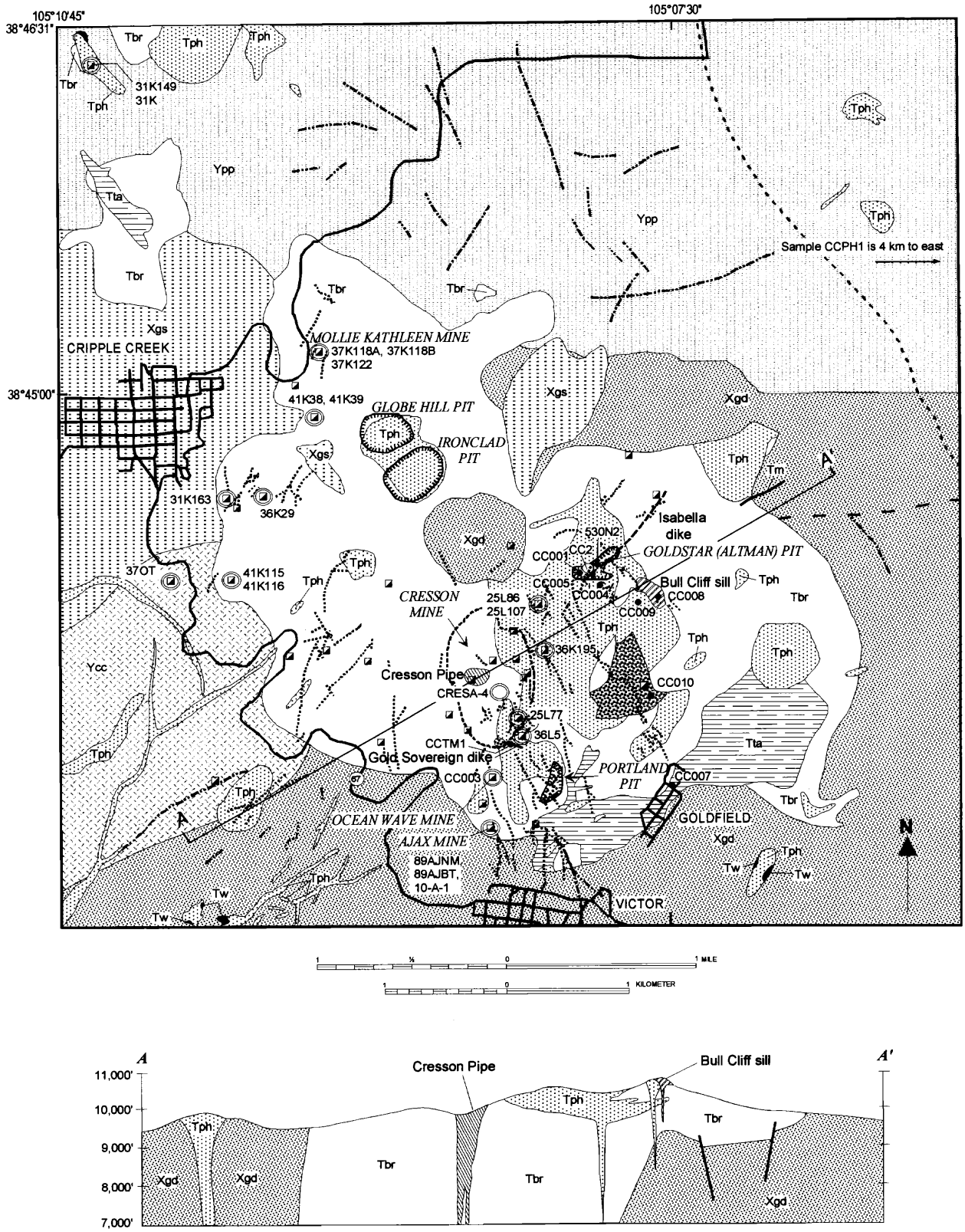

FIG. 2. Geologic map of the Cripple Creek district (modified from Birmingham, 1987; and Pontius, 1996) showing locations of samples used in this study.

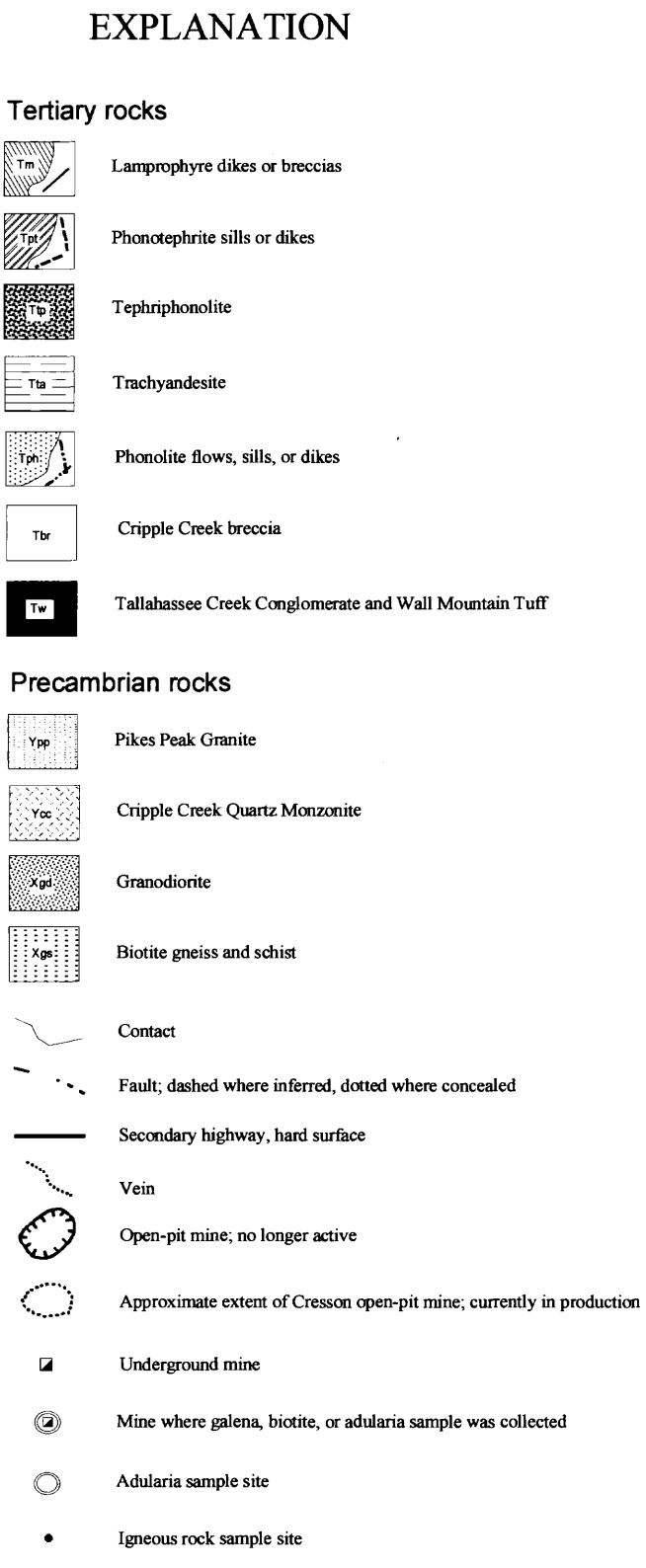

FIG. 2. (*Cont.*)

rocks are overlain by typical Cripple Creek breccia, and fragments of the sedimentary rocks are present in the breccia (Thompson et al., 1985). The sediments appear to have been transported by fluvial processes into a shallow lacustrine environment. Evidence for this includes crossbedded sandstones, ripple-laminated siltstones, fossil leaves, dessication cracks, and bird footprints (Koschmann, 1949; Thompson et al., 1985) in beds that are continuous for significant horizontal distances (possibly up to 800 m), particularly in the eastern part of the complex (Loughlin and Koschmann, 1935).

The Cripple Creek breccia was intruded by dikes and irregular masses of alkaline igneous rocks, mostly in the southern and eastern parts of the complex (Fig. 2). Dikes, plugs, and flows also occur outside the complex within a distance of about 12 to 15 km. Outside the complex, the alkaline igneous rocks cut or overlie either Precambrian rocks or Oligocene Tallahassee Creek Conglomerate or Wall Mountain Tuff (Fig. 2).

The most voluminous igneous rocks are phonolite (Tph, Fig. 2), with lesser amounts of more mafic rocks such as tephriphonolite and trachyandesite (Ttp and Tta). Mafic and ultramafic alkaline lamprophyric rocks (Tm), primarily monchiquite and vogesite, are also common throughout the complex but are volumetrically the least important. A few are exposed at the surface (Fig. 2), but most are known from underground mapping (Lindgren and Ransome, 1906; Loughlin and Koschmann, 1935).

Origin and development of the complex

There are conflicting interpretations about the origin and development of the Cripple Creek complex. The earliest interpretations by Cross and Penrose (1895), Lindgren and Ransome (1906), and Loughlin and Koschmann (1935) were that the volcanic "crater" was produced by a succession of violent volcanic eruptions. However, in subsequent field work, Koschmann (1949) noted the horizontal and vertical extent of volcanic and nonvolcanic rocks which earlier had been attributed to sedimentation in the crater following explosive activity. Even at depths as great as 1,000 m below the surface, waterlain volcanic sediments were encountered (Koschmann, 1949). These observations led to the conclusion that subsidence, and not explosive volcanism, was the primary process responsible for the initial formation of the complex (Koschmann, 1949).

Although the emplacement history is still not completely understood, most recent workers agree that the initial activity involved eruptive volcanism and diatreme development. This was followed by a long period of fluvial and lacustrine sedimentation and subsidence that was interrupted by intrusion, brecciation, and diatreme emplacement (Thompson et al., 1985; Thompson, 1992; Pontius, 1996). Southwest of Victor, the Oligocene Tallahassee Creek Conglomerate underlies phonolite (Fig. 2), indicating that a paleovalley or local basin existed prior to eruption of Cripple Creek volcanic rocks. Phreatomagmatic eruptions may have initiated small eruptive centers or diatremes when magmas ascending along zones of weakness associated with the northwest-trending structural zones, encountered water within fractured granite or in saturated Tallahassee Creek Conglomerate (Birmingham, 1987; Pontius, 1996). As the eruptive centers enlarged, subsidence locally became prominent. Shallow bodies of water were present into which ash and fluvially transported conglomeratic and pyroclastic sediments were deposited (Thompson et al., 1985). Sedimentation was interrupted periodically by intrusion of alkaline magmas; those that encountered little or no

water formed dikes, stocks, and/or surface flows, whereas those that encountered abundant water produced phreatic explosions resulting in small diatremes.

Mineral Deposits

There are two primary styles of mineralization in the Cripple Creek district: high-grade gold-telluride veins and low-grade disseminated gold and pyrite deposits. Most of the 21 Moz of past production has come from the high-grade vein deposits. Recent exploration (since 1989) has delineated low-grade, near-surface, disseminated gold deposits that occur as broad zones in permeable rocks within the upper 300 m of the diatreme complex (Pontius, 1996). Most of this mineralized rock is contained within the Cresson deposit. A proven and probable reserve of over 104 t of gold (3.7 Moz) with an additional drill-indicated resource base of nearly 60 t (2.1 Moz) have been added to the district resource as a result of the recent exploration. Approximately 450,000 oz of gold has been mined from the Cresson open-pit mine since production began in February 1995 (76,500 oz in 1995; 174,000 oz in 1996, and 198,000 oz in 1997).

Vein deposits

The majority of the historically productive high-grade veins cut Precambrian crystalline rocks and Tertiary rocks and are radially distributed throughout the complex (Fig. 2). Most of the gold came from gold- and gold-silver-bearing telluride minerals. The average gold/silver ratio for the district is about 9/1, although the ratio for select veins can range widely (e.g., the Bobtail vein in the Ajax mine ranges from 1/5 up to 23/1; Thompson et al., 1985).

The veins are not filled with massive quartz as is common with many epithermal gold deposits. Instead, they typically display an open vuggy structure (Lindgren and Ransome, 1906). They form sheeted zones that consist of a number of narrow (<50 mm) subparallel fissures, which collectively form a lode ranging from 0.5 to 3 m in width (Lindgren and Ransome, 1906). Typically, the sheeted zones are parallel to and occur within or immediately adjacent to mafic phonotephrite or phonolite dikes. The vein systems are most extensively developed at the surface, but with increasing depth (from 600–1,000 m), the veins are less abundant and narrower (Koschmann, 1949). The most productive gold mines are located where northwest- and northeast-trending vein systems intersect. For example, the Portland and Goldstar (Altman) open-pit mines are located at the intersection of northwest- and northeast-trending vein systems (Koschmann, 1949).

High-grade gold-telluride deposits also occur as open-space fillings within discordant diatreme breccias (Loughlin and Koschmann, 1935). The Cresson blowout or pipe is an unusual breccia in the form of a pipe-shaped body that occurs in the south-central part of the complex. The breccia is composed of fragments of Precambrian rocks and alkaline igneous rocks, including mafic lamprophyric rocks, that are set in a matrix of lamprophyre and fine-grained fragmental material. Parts of the Cresson pipe are highly mineralized. One vug, measuring 12 m high, 6 m long, and 4.5 m wide, produced 58,055 oz of gold within four weeks of its discovery (Smith et al., 1985; Nelson, 1989). At this locality, gold- and gold-silver-bearing tellurides, and native gold filled open spaces between fragments in the breccia body.

The most common ore mineral in the vein systems and in the open-space fillings is calaverite ($AuTe_2$) with lesser amounts of krennerite [$(Au,Ag)Te_2$], sylvanite [$AuAgTe_4$], and petzite [Ag_3AuTe_2] (Lindgren and Ransome, 1906; Saunders, 1986). The most common sulfide is pyrite, although sphalerite and galena are also typically associated with gold tellurides. Molybdenite is rarely intergrown with pyrite, sphalerite, and galena (Lindgren and Ransome, 1906). Tetrahedrite occurs throughout the district and at all levels and is commonly intergrown with calaverite. Stibnite is associated with gold ores at high-level vein exposures (Lindgren and Ransome, 1906). Other sulfide minerals such as chalcopyrite and cinnabar have been reported in one or two localities (Dwelley, 1984; Saunders, 1986) but generally are rare in the district. Native gold is present locally, as a product of oxidation of gold tellurides (Lindgren and Ransome, 1906) and rarely as a hypogene mineral that is paragenetically late (post-telluride mineralization; Lindgren and Ransome, 1906; Saunders, 1986).

The mineral paragenesis of the vein deposits has been previously described (Lindgren and Ransome, 1906; Loughlin and Koschmann, 1935; Thompson et al., 1985). A generalized district-wide three-stage mineral paragenesis was recognized by Lindgren and Ransome (1906) and Loughlin and Koschmann (1935). From oldest to youngest these stages are: (1) quartz, biotite, K feldspar, dark purple fluorite, dolomite, and coarse-grained pyrite; (2) milky to smoky quartz, lighter colored purple fluorite, fine-grained pyrite, dolomite, ankerite, celestite, barite, molybdenite, sphalerite, galena, tetrahedrite, roscoelite, and telluride minerals (telluride mineral deposition was consistently later than base metal sulfides); and (3) native gold, smoky to colorless quartz, fluorite, chalcedony, fine-grained pyrite, and calcite.

Although the ore and gangue mineralogy of each stage is generally consistent throughout the vertical extent of each vein system (i.e., there is little vertical mineralogical or geochemical zoning over the 1,000-m extent of the veins), the proportions of each stage vary between individual veins as well as within veins (Lindgren and Ransome, 1906; Thompson et al., 1985). Only a few vein samples display all stages (Fig. 3A). More typical are veins that contain two or more minerals of the early quartz-biotite-K feldspar-fluorite-dolomite-pyrite assemblage, followed by deposition of base metal sulfide minerals without significant telluride mineral deposition (Fig. 3B), or quartz veins with calaverite with no base metal sulfides (Lindgren and Ransome, 1906; Fig. 3C). Also present are veinlets and veins containing intergrown biotite, K feldspar, and pyrite without other gangue or ore minerals. These have been observed from the Mollie Kathleen (Fig. 3D), Ocean Wave, and Dolly Varden mines (Lindgren and Ransome, 1906). Pyrite from one of these veinlets (the Dolly Varden mine) reportedly was auriferous, grading 0.08 oz/t (Lindgren and Ransome, 1906).

Vein-related hydrothermal alteration is most extensive in porous and permeable rocks of the Cripple Creek breccia, although alkaline igneous rocks of all compositions may be altered to some extent, particularly the more mafic ones (Lindgren and Ransome, 1906). Vein-related alteration is dependent on vein type and can occur as widespread halos

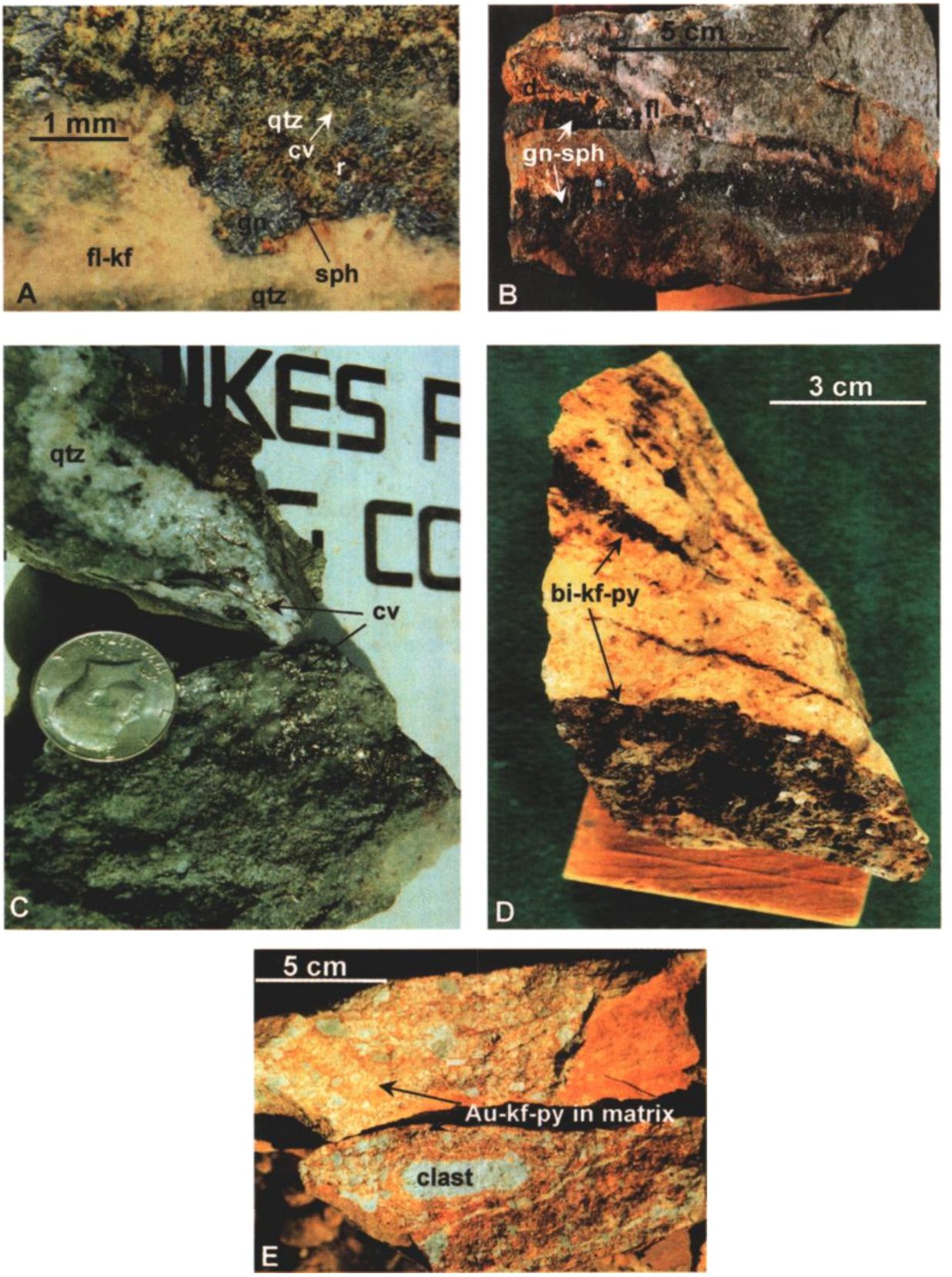

FIG. 3. Photographs of mineralized rocks from vein and disseminated deposits. A. Vein showing all three primary stages, including early quartz-fluorite-K feldspar (qtz-fl-kf), followed by galena and sphalerite (gn-sph), and finally calaverite (cv) and quartz (qtz). Green roscoelite (r) formed as a gangue mineral immediately preceding calaverite deposition. B. Vein with early fluorite (fl), followed by deposition of sphalerite and galena (sph-gn) with late dolomite (d). Telluride minerals are absent. C. Quartz vein with calaverite. D. Veinlets of biotite, K feldspar, and pyrite (bi-kf-py) in altered phonolite. E. Native Au, pyrite, and K feldspar in matrix of breccia from the Cresson deposit.

surrounding K feldspar-pyrite veins (Jensen and Barton, 1997). However, alteration that envelopes the telluride veins typically occurs in a narrow selvage that extends outward to no more than 5 × the vein width (Thompson et al., 1985). Alteration products include pyrite, sericite, roscoelite, adularia, dolomite, magnetite, and fluorite (Lindgren and Ransome, 1906; Thompson et al., 1985).

Primary fluid inclusions in quartz and fluorite from the Newmarket and Bobtail veins in the Ajax mine (Dwelley, 1984) show that early-stage fluids (quartz-biotite-K feldspar-fluorite-dolomite-pyrite) were hot (avg 250°C; Thompson, 1996). Gold-telluride precipitation in veins from the Ajax mine was interpreted by Dwelley (1984) to have come from relatively cooler (105°–159°C) fluids. Similarly, fluid inclusion studies on samples from the Cresson deposit revealed that hydrothermal solutions from which telluride precipitation occurred were low temperature (131°–175°C) and low-salinity (3–9.6 wt % NaCl equiv), neutral to alkaline (pH 5–6), relatively oxidized fluids (Saunders, 1986).

Disseminated deposits

Recent exploration has delineated previously undocumented low-grade, near-surface disseminated gold deposits within the Cripple Creek district (Fig. 3E). These deposits occur as broad zones within the upper 300 m of the complex (Pontius, 1996). The best-developed deposits are confined to structural intersections or along the major northwest-trending shear zones (Pontius, 1996). The Cresson deposit, which is currently being mined, is the largest deposit of this type. This should not be confused with the historic Cresson mine, which was located in the vicinity of the disseminated Cresson deposit, but which was a telluride-dominant open-space vug and vein system (Loughlin and Koschmann, 1935; Saunders, 1986).

Typically, the gold occurs as microcrystalline native Au and Au-bearing pyrite (Pontius, 1996). Gangue minerals include fluorite, quartz, barite, and dolomite. Alteration associated with disseminated deposits produced primarily K feldspar and pyrite in the form of pervasive flooding of fine-grained K feldspar, along with moderate to strong sericitization with euhedral fine- to medium-grained pyrite (Burnett, 1995; Pontius, 1996).

Methods

Samples of igneous rocks were collected from surface outcrops within and outside the Cripple Creek complex in order to investigate the petrology, geochemistry, and geochronology. Although attempts were made to collect the least altered rocks, thin section petrography revealed that the rocks are variably altered. In most cases, this alteration consists of partial replacement of feldspar or biotite phenocrysts by clays or chlorite, respectively. Groundmass minerals are largely unaltered in felsic end members, whereas alteration minerals occur in the groundmass of the relatively more mafic rocks.

Where possible, igneous rock samples were collected from the same sample locations as those used by Birmingham (1987). This was to assure that the mineralogy and textural relationships of the rocks collected during this study are consistent with those from Birmingham (1987) so that geochemical and isotopic data obtained during this study could be compared to previously obtained data.

Some mineralized vein samples were also collected from surface exposures, but the majority were obtained from the Koschmann Collection, consisting of over 1,000 samples collected by A.H. Koschmann and G.F. Loughlin from now inaccessible underground mines. Samples were keyed to original field notes, obtained at the archive library of the U.S. Geological Survey and to field maps of underground mines (Koschmann and Loughlin, 1965).

To obtain mineral separates for isotopic studies, rocks were crushed and sieved to recover the 125- to 250-μm fraction and then separated using heavy liquids and a Frantz isodynamic separator. If necessary, mineral separates were handpicked to greater than 99 percent purity.

Major and trace element analyses were obtained at the laboratories of the U.S. Geological Survey in Denver, Colorado. Major element compositions were obtained by X-ray fluorescence analysis following the method of Taggart et al. (1987). Trace element compositions were measured by inductively coupled plasma atomic emission spectrometry (ICP-AES) and inductively coupled plasma mass spectrometry (ICP-MS) using the methods of Crock et al. (1983) and Meier et al. (1994). Fluorine was determined by the ion-selective electrode potentiometric method (O'Leary and Meier, 1986), and Au, Te, and Tl were analyzed by flame atomic absorption (Hubert and Chao, 1985).

Lead isotope compositions were determined with an NBS solid-source mass spectrometer at the U.S. Geological Survey in Denver, Colorado. The raw lead isotope data were adjusted to absolute values by mass discrimination fractionation factors determined by repeated analyses of interlaboratory common lead standard NBS SRM 981 (Catanzaro et al., 1968). Oxygen and hydrogen were extracted from mineral separates using standard procedures described in Godfrey (1962) and Taylor and Epstein (1962a).

The $^{40}Ar/^{39}Ar$ analyses were done at the U.S. Geological Survey in Denver, Colorado, using procedures described in Dalrymple et al. (1981) and Snee et al. (1988). The flux monitor used was hornblende Mmhb-1 with a K/Ar age of 520.4 ± 1.7 Ma (Alexander et al., 1978). The samples were irradiated at the TRIGA reactor at the U.S. Geological Survey. Isotopic abundances were measured using a Mass Analyzer Products 215 Series Rare Gas mass spectrometer. Corrections for interfering isotopes were also made; corrections for Cl-derived ^{37}Ar were determined using the method of Roddick (1983). Production ratios measured on pure K_2SO_4 and CaF_2 salts irradiated with the samples were used to correct for irradiation-produced ^{40}Ar (from K) and ^{39}Ar (from Ca).

Petrogenesis of the Igneous Rocks

Petrography and mineralogy

Classification of the Cripple Creek igneous rocks was originally based on petrographic descriptions and whole-rock chemical analyses (Lindgren and Ransome, 1906; Eriksson, 1987). Using the total alkali-silica diagram (Le Bas et al., 1986), the rocks were subsequently reclassified (Birmingham, 1987) as a suite of rocks ranging in composition from ultramafic and mafic rocks, such as lamprophyre and phonotephrite, to tephriphonolite, trachyandesite, and phonolite (Figs. 4 and 5). A comparison of rock names used by Lindgren and Ransome (1906) and the new alkali-silica classification is shown in Table 1.

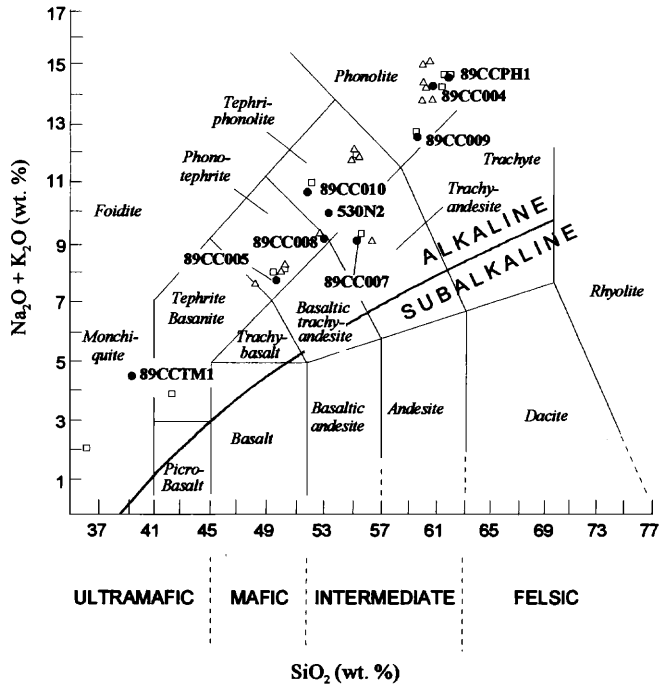

FIG. 4. Total alkali-silica diagram (Le Bas et al., 1986), showing compositions of unaltered igneous rocks from the Cripple Creek district. All data are calculated volatile free. The line from Irvine and Baragar (1971) separates alkaline from subalkaline rocks. Solid circles are samples from this study (data are listed in Table 2). Also shown for comparison are samples from previous studies: open triangles are samples from Lindgren and Ransome (1906); open squares are samples from Birmingham (1987).

The greatest volume of igneous rocks is inside the complex (Fig. 2). Phonolite (Tph) comprises the largest volume of rock (about 90%), with tephriphonolite (Ttp), trachyandesite (Tta), and late mafic and ultramafic rocks (Tpt and Tm, respectively) comprising the remainder, in roughly equal proportions (Fig. 2). Dikes and sills of phonolite are the only igneous rocks found in significant volumes outside the complex.

Phonolite is typically gray-green, but alteration has resulted in colors ranging from light gray to white, or maroon to brown. The phonolite is primarily holocrystalline-aphanitic, although porphyritic textures are locally present. Alkali feldspar is the most common mineral, both as phenocrysts and in the groundmass. Other minerals include plagioclase, clinopyroxene (aegerine-augite), analcime, sodalite, and nosean. Accessory minerals in the phonolite are brown amphibole, titanite, apatite, titanomagnetite, hematite, ancylite, betafite, fluorite, pyrite, rutile, and zircon (Birmingham, 1987).

Tephriphonolite is a light to dark gray porphyritic rock that is mineralogically similar to phonolite, except it contains more clinopyroxene and plagioclase and less sanidine. Biotite and brown amphibole are relatively more common, and feldspathoid minerals are present in roughly equal proportions in both rock types (Birmingham, 1987; Kelley, 1996). Accessory minerals include rare olivine (Fo_{74}), apatite, titanite, titanomagnetite, zirkelite, ferroan magnesiochromite, zircon, and calcite (Birmingham, 1987).

Dark gray to black phonotephrite forms aphanitic sills (Bull Cliff sill) and porphyritic dikes (Isabella dike) in the eastern part of the complex. Plagioclase and clinopyroxene (salite) are the most common minerals in the phonotephrite, but feldspathoid minerals (analcime and sodalite), biotite, and rare olivine are also present (Birmingham, 1987). The most abundant accessory mineral is titanomagnetite which is widely distributed in the groundmass. Apatite, baddeleyite, and zirkelite were also identified (Birmingham, 1987). Brown and bluish green amphibole were reported in some porphyritic phonotephrite dikes (Lindgren and Ransome, 1906).

Trachyandesite occurs along the southeastern margin of the complex (Fig. 2) and was previously mapped as latite phonolite (Lindgren and Ransome, 1906), but due to quartz in late cavities between phenocrysts, it was renamed trachyandesite (Birmingham, 1987). It is a medium gray to brownish porphyritic rock with phenocrysts of plagioclase, clinopyroxene, and biotite in a groundmass of feldspar, apatite, titanite, and iron oxides. Plagioclase is the most common phenocryst mineral, but clinopyroxene and flakes of biotite are also common. Lindgren and Ransome (1906) reported the presence of sodalite and nosean.

Two types of lamprophyre, monchiquite and vogesite, were recognized by Lindgren and Ransome (1906). Monchiquite is the most common and is best exposed at the surface as the Gold Sovereign dike in the south-central part of the complex (Fig. 2). It also occurs as fragments in the Cresson diatreme. Monchiquite is a dark greenish gray to black porphyritic rock with abundant olivine as large rounded crystals or locally as small anhedral crystals in the groundmass. Large flakes of phlogopite and clinopyroxene up to 2 to 3 mm across are also present. Groundmass minerals in monchiquite include clinopyroxene, analcime, and hauyne.

Vogesite dikes are relatively rare and are poorly characterized. Most reported occurrences are from subsurface exposures, with the exception of the Pinto vogesite dike exposed in the Goldstar (Altman) open-pit mine. The Pinto dike is extremely altered except for the presence of apparently fresh phlogopite.

Major and trace element geochemistry

Major element geochemical data for phonolite, tephriphonolite, phonotephrite, trachyandesite, and lamprophyre collected within and outside the complex show that Cripple Creek igneous rocks have high alkali contents ($Na_2O + K_2O > 4.1$; Fig. 4) and are consistently Na rich relative to K (Table 2). In general, the major element variations show coherent trends and a relatively continuous chemical progression from phonotephrite through phonolite, with a large compositional gap between phonotephrite and lamprophyre (Fig. 6). In general, there are systematic decreases in CaO, MgO, and TiO_2 and increases in Al_2O_3, K_2O, and Na_2O with increasing SiO_2 from phonotephrite to phonolite. These trends in major element concentrations are consistent with fractional crystallization of early plagioclase and ferromagnesian and oxide minerals and the late appearance of K feldspar as primary phases.

Trace element compositions also show systematic variations that are consistent with fractional crystallization. For instance, compatible elements (mineral-melt distribution coefficients >1) like Sc, Cr, and Ni initially decrease strongly from lamprophyre to phonotephrite, with very low concentrations in the most evolved rocks (Table 2; Fig. 7). In contrast, elements such as Nb, U, and Th increase gradually in mafic to interme-

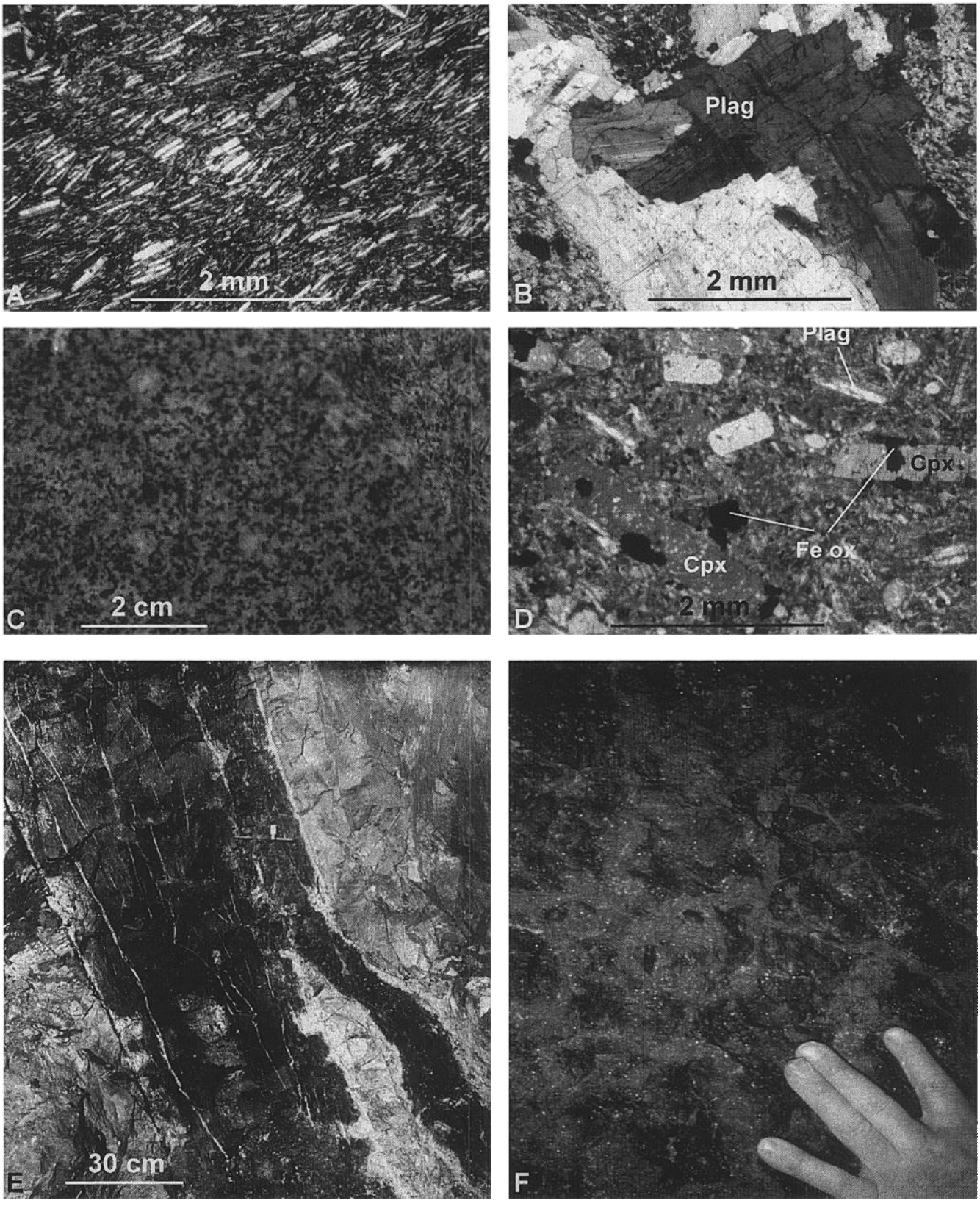

FIG. 5. Examples of igneous rocks from the Cripple Creek district. A. Photomicrograph in transmitted light of phonolite showing trachytic texture of primarily sanidine (light mineral) and clinopyroxene (dark mineral; sample CCPH1). B. Photomicrograph in transmitted light of porphyritic plagioclase-bearing phonolite (sample CC009). C. Hand sample of tephriphonolite (sample CC010) showing equigranular nature of clinopyroxene, biotite (dark minerals), plagioclase, and sanidine (light minerals). D. Photomicrograph in transmitted light of phonotephrite (Isabella dike; sample CC005) showing

TABLE 1. Rock Names Assigned Using the Total Alkali-Silica Igneous Classification System Compared with Previous Classification by Lindgren and Ransome (1906)

Previous classification	Total alkali-silica classification
Phonolite	Phonolite
Latite-phonolite	Phonolite
Syenite	Tephriphonolite
Trachydolerite	Phonotephrite
Trachybasalt	Phonotephrite

diate compositions, followed by rapid increases and extreme enrichments in the most evolved rocks. Chondrite-normalized REE patterns have steep negative slopes and are light REE enriched (La/Yb_{cn} = 28–50), with phonolite showing the most extreme enrichment (La about 680 × chondrite values; Fig. 8A). In addition, there is a distinct depletion in middle REE in tephriphonolite and phonolite relative to more mafic rocks, suggesting the importance of apatite and titanite fractionation.

A chondrite-normalized spider diagram shows that the rocks are enriched in incompatible and low field strength elements (Ba, Th, U, Sr) and depleted in Ti and Y compared to intraplate alkaline basalt (OIB; Fig. 8B). In the mafic and ultramafic rocks, K is strongly depleted relative to U and Nb. The pattern for evolved phonolite (CCPH1; Fig. 8B) shows extreme depletions in Ba, Sr, and Ti due to the nearly complete fractionation of plagioclase and titanite. The Ba/La, La/Nb, and Zr/Nb ratios of the Cripple Creek rocks (Table 2) are typical of intraplate alkaline magmas (i.e., OIB basalts have Ba/La < 15, La/Nb < 2, Zr/Nb < 20; Wilson, 1989).

The mineralogical trends and regularity of chemical patterns argue for differentiation of the trachyandesites, tephriphonolites, and phonolites through fractional crystallization of phonotephrite. However, there are apparent problems with this model when the timing of eruption or intrusion of the different rock types and their relative abundances are considered. As noted earlier, emplacement of phonotephrite dikes occurred after emplacement of the felsic phonolitic rocks, and the phonolites far exceed the basaltic and intermediate rocks in abundance. This implies that the phonotephrite cannot be parental to the intermediate and felsic rocks as might be inferred from previous discussions. However, for other volcanic districts such as the East African rift, similar relationships between ages and abundances of different rock types have been explained by invoking a large magma chamber beneath the rift, with eruptive centers situated above cupolas on this magma chamber (Weaver et al., 1972). It is possible that through the eruptive history of any one of these volcanoes, effusive activity never exceeded the rate at which differentiation was producing phonolite in the cupola, so that mafic rocks were rarely erupted, and then only in small amounts.

A similar magma chamber may have existed below Cripple Creek. Mantle-derived basaltic magmas rising beneath rift axes tend to pond beneath the crust, leading to development of lensoid bodies (Wilson, 1989). Hermance (1982) has suggested that a low resistivity zone at a 20- to 40-km depth (i.e., near lower crustal-mantle depths) may represent a zone of magma accumulation beneath the Rio Grande rift. Wendlandt et al. (1991) provided isotopic constraints that support this magmatic underplating of the lower crust. These data suggest that accumulations of magma may exist beneath or within the crust of the Rio Grande rift. Such a pool of alkali basalt magma at the base of the crust could supply over time individual batches of magma which could ascend along structures to shallow depths where they might undergo differentiation and ultimately be extruded. Such a model can explain the lack of early basaltic volcanism.

In spite of these arguments, it is perhaps more likely that alkali basaltic magmas were injected in pulses and that the phonotephrites and lamprophyres at Cripple Creek were a late pulse after a main stage of emplacement and fractionation. The similarity in spider diagram patterns for lamprophyre and phonotephrite, and the fact that they appear to be intimately related in time, would suggest a genetic relationship between lamprophyre and phonotephrite. The lamprophyres may represent the tapping of a new enriched mantle source region that perhaps evolved through fractionation and assimilation of lower crustal rocks to produce the phonotephrite.

Oxygen isotope geochemistry

The $\delta^{18}O$ values for mineral separates from igneous rocks (Table 3) show that magnetite has $\delta^{18}O$ values that are equal to or less than clinopyroxene, which in turn are less than feldspar (Table 3; Fig. 9). The order of increasing $\delta^{18}O$ values from magnetite to feldspar is consistent with the order expected for a suite of related igneous rocks (Taylor and Sheppard, 1986). The clinopyroxene and feldspar separates from Cripple Creek have $\delta^{18}O$ values typical of unaltered alkaline rocks. For example, $\delta^{18}O_{pyroxene}$ values typically range from 5.5 to 6.6 per mil in syenites and 4.9 to 5.6 per mil in mafic igneous rocks (Taylor et al., 1967; Anderson et al., 1971; Taylor and Sheppard, 1986), whereas values for feldspars in syenites and phonolites range from 6.6 to 7.6 and 6.6 to 8.0 per mil, respectively (Taylor et al., 1967; Taylor and Sheppard, 1986; Wörner et al., 1987).

The $\delta^{18}O$ values of feldspar from igneous rocks can also be used to place limits on the $\delta^{18}O$ values of the magma (Taylor and Sheppard, 1986). Plagioclase and potassium feldspar in the Cripple Creek rocks display a relatively restricted range in $\delta^{18}O$ values and therefore were used to calculate whole-rock or magma compositions (Table 3). As expected, there is an overall increase in $\delta^{18}O_{magma}$ values with increasing differentiation throughout the suite. Phonotephrite has the lowest values (6.4 and 7.1‰), and tephriphonolite, trachyandesite, and phonolite have relatively higher values (7.7–8.4‰). These values are similar to alkaline igneous rocks from other regions throughout the world (Taylor, 1968; Kyser et al., 1982; Wörner et al., 1987).

phenocrysts of clinopyroxene (cpx) and plagioclase (plag) with abundant Fe-Ti oxides. E. Phonotephrite dike from the Portland mine, level 5, showing platy parting. Seams are filled with calcite (photograph by F.L. Ransome, 1901). F. Photograph of the Trail diatreme breccia pipe, a lamprophyre of monchiquite composition (photograph by J.A. Pontius, 1995).

TABLE 2. Representative Major (wt %) and Trace (ppm) Element Analyses of Least Altered Igneous Rocks from the Cripple Creek District

Sample no.	CC004 (1)	CCPH1 (1)	CC009 (1)	CC007 (2)	530N2 (3)	CC010 (3)	CC005 (4)	CC008 (4)	CCTM1 (5)
SiO_2	59.1	60.0	57.9	53.0	51.6	50.0	47.9	51.3	36.5
TiO_2	0.34	0.20	0.65	1.20	1.29	1.26	1.49	1.24	1.90
Al_2O_3	19.6	19.7	19.4	17.4	18.7	18.5	16.1	18.1	10.9
Fe_2O_3	1.93	1.76	2.00	4.19	3.69	3.64	4.83	4.61	4.82
FeO	0.65	0.36	1.36	2.32	3.30	3.04	3.91	2.57	5.38
MnO	0.24	0.20	0.17	0.19	0.17	0.17	0.24	0.19	0.19
MgO	0.31	0.15	0.72	2.14	2.09	2.59	4.55	2.55	14.3
CaO	1.25	0.65	2.83	6.04	5.73	6.18	8.69	6.51	13.8
Na_2O	8.26	8.83	6.89	5.09	4.99	5.95	3.98	4.94	2.96
K_2O	5.72	5.45	5.41	3.69	4.38	4.52	3.56	4.01	1.18
P_2O_5	0.06	<0.05	0.20	0.57	.52	0.59	0.81	0.72	1.26
H_2O^+	0.44	0.67	0.38	0.90	1.7	1.66	1.70	1.95	2.88
H_2O^-	0.31	0.25	0.13	0.29	0.19	0.25	0.35	0.33	0.75
CO_2	0.03	<0.01	0.08	1.91	0.01	0.02	1.09	0.67	0.34
Total	98.2	98.3	98.1	98.9	98.4	98.4	99.5	99.0	97.2
Mg#[1]	21	14	32	42	44	46	53	44	75
$Na_2O + K_2O$	14.0	14.3	12.3	8.78	9.37	10.5	7.54	8.95	4.14
K_2O/Na_2O	0.69	0.62	0.78	0.72	0.88	0.76	0.89	0.81	0.39
As	0.89	4.5	0.63	N	NA	N	N	N	0.14
Au	N	N	N	N	NA	0.004	0.004	N	0.004
Ba	360	23	1,600	1,800	NA	1,800	1,400	1,900	1,500
Ce	320	230	280	300	NA	230	210	250	230
Co	1	<1	5	15	NA	20	33	19	59
Cr	3	1	<1	9	NA	13	59	4	340
Cu	4	6	5	17	NA	39	70	13	81
Dy	4.3	2.7	5.5	8.1	NA	5.3	5.9	6.3	5.3
Er	3.2	2.4	3.1	3.5	NA	2.3	2.5	2.9	2.0
Eu	1.4	0.61	2.8	4.3	NA	3.7	3.5	3.7	4.6
F	0.11	0.10	0.10	0.06	NA	0.09	0.07	0.08	0.09
Gd	4.6	1.8	6.3	10	NA	7.5	8.7	8.9	10
Ho	0.90	0.59	1.0	1.4	NA	0.92	1.0	1.2	0.93
La	250	200	180	180	NA	140	120	140	120
Mo	4	3.1	5.3	2.1	NA	2.4	0.6	3.5	3.1
Nb	150	130	110	70	NA	84	42	66	47
Nd	31	37	89	110	NA	86	89	100	110
Ni	<2	<2	<2	5	NA	11	22	3	280
Pb	30	49	20	14	NA	15	14	11	13
Pr	22	15	25	30	NA	22	22	26	26
Rb	200	230	126	70	NA	70	90	50	65
Sc	<2	<2	<2	7	NA	8	17	6	25
Sm	6.2	3.1	9.8	15	NA	11	12	13	15
Sr	300	18	1,300	2,100	NA	1,800	1,700	2,200	2,400
Tb	0.74	0.43	1.2	1.6	NA	1.1	1.2	1.4	1.4
Te	N	N	N	N	NA	N	N	N	N
Th	90	116	46	33	NA	35	26	21	21
Tl	0.5	1.0	0.35	0.2	NA	N	0.9	0.2	1.0
Tm	0.62	0.45	0.44	0.45	NA	0.38	0.36	0.40	0.21
U	13	29	9	5	NA	6	6	5	4
V	24	21	54	120	NA	160	210	150	280
Y	28	19	28	33	NA	23	25	30	20
Yb	5.0	4.0	3.6	3.1	NA	2.4	2.8	2.4	1.6
Zn	160	150	100	110	NA	100	140	110	110
Zr	850	1,000	323	172	NA	251	220	282	182
Ba/La	1.44	0.12	8.9	10	NA	12.9	11.7	13.6	12.5
La/Nb	1.7	1.5	1.6	2.6	NA	1.7	2.9	2.1	2.6
Zr/Nb	5.7	7.7	2.9	2.5	NA	2.9	5.2	4.3	3.9
Sr/Nd	9.7	0.48	14.7	19.1	NA	21.0	19.1	22.0	21.8
Rb/Sr	0.7	12.8	0.1	0.03	NA	0.04	0.05	0.02	0.03

Samples: (1) = phonolite, (2) = trachyandesite, (3) = tephriphonolite, (4) = phonotephrite, (5) monchiquite
NA = not analyzed, N = not detected at lower limit of detection
[1] Mg# = 100 $Mg^{2+}/Fe^{2+} + Mg^{2+}$
$Fe^{2+}/(Fe^{3+} + Fe^{2+}) = 0.87$ (Carmichael and Ghiorso, 1986)

Oxygen isotope variations in igneous rocks can be used to semiquantitatively predict the effects of fractional crystallization and assess the importance of crustal contamination in the evolution of continental volcanic suites. A variation of approximately 1 per mil in a suite of comagmatic rocks has been used by Taylor and Epstein (1962b) to indicate that

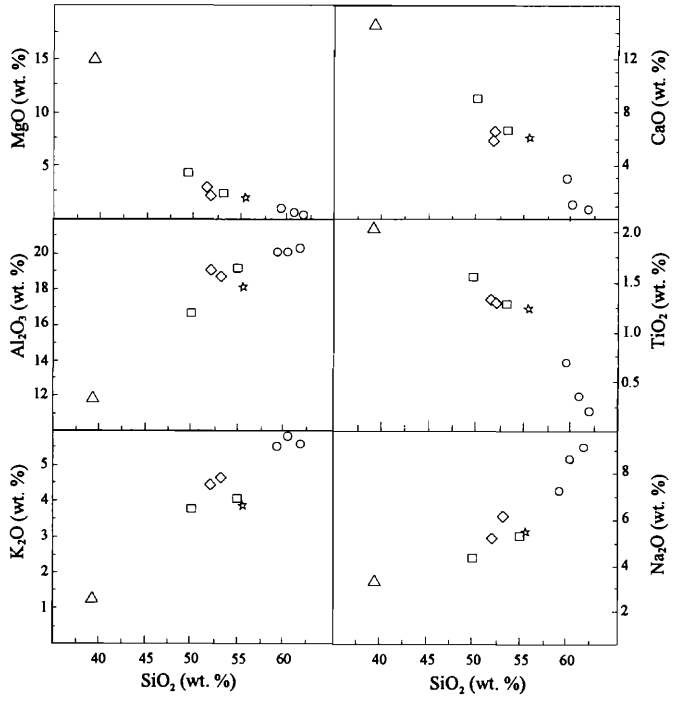

FIG. 6. Harker diagrams showing variations in MgO, CaO, Al_2O_3, K_2O, Na_2O, and TiO_2 vs. SiO_2 for unaltered lamprophyre (triangle), phonotephrite (square), tephriphonolite (diamond), trachyandesite (star), and phonolite (circle) in the Cripple Creek district. Note the relatively continuous progression from phonotephrite through phonolite for all elements. Note also the compositional gap between lamprophyre and other rocks.

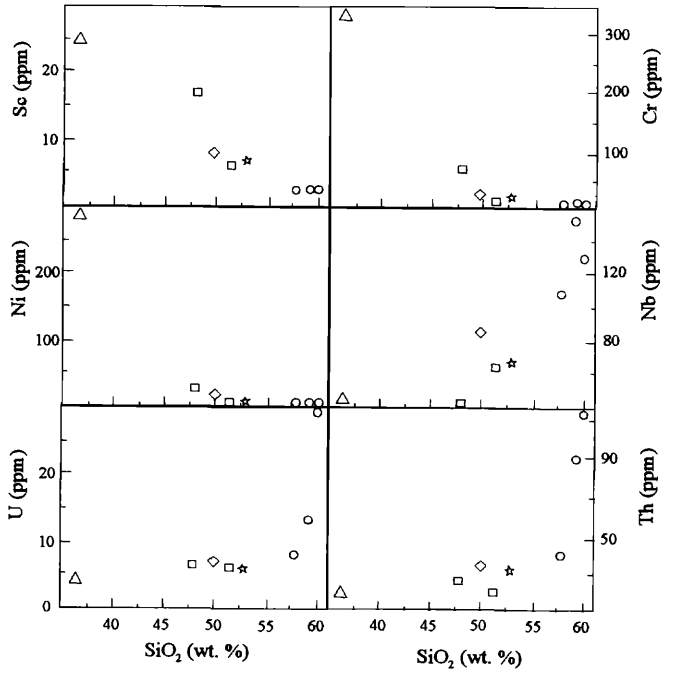

FIG. 7. Diagrams showing variations in Sc, Cr, Ni, Nb, U, and Th vs. SiO_2 for unaltered lamprophyre (triangle), phonotephrite (square), tephriphonolite (diamond), trachyandesite (star), and phonolite (circle) in the Cripple Creek district.

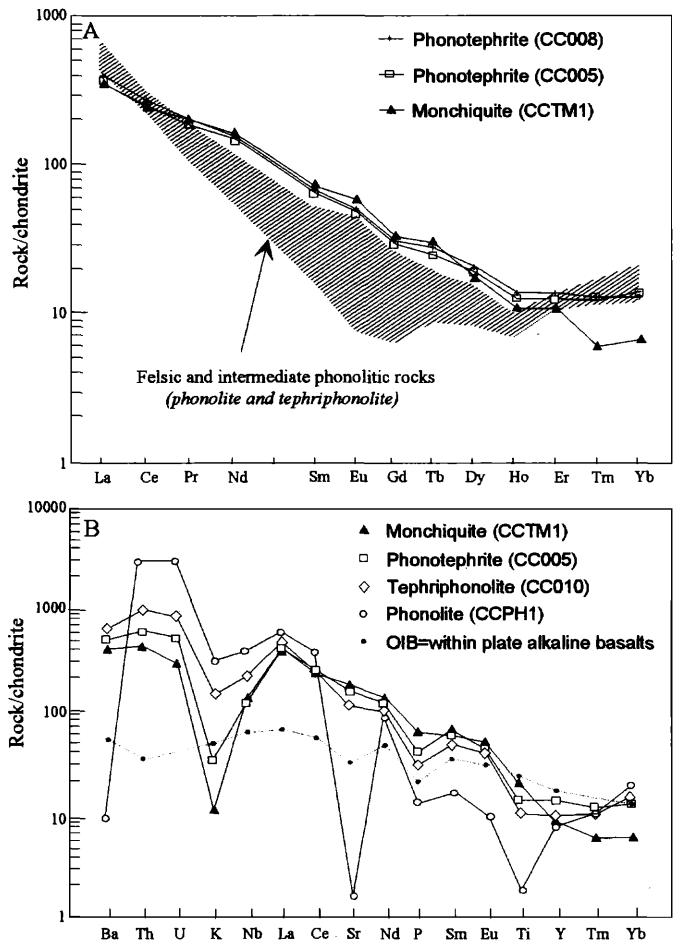

FIG. 8. A. Chondrite-normalized rare earth element (REE) plots of lamprophyre and phonotephrite. The ranges of relatively more evolved rocks are shown for comparison. Normalization values of Taylor and McLennan (1985). B. Spider diagrams for unaltered monchiquite, phonotephrite, tephriphonolite, and phonolite from the Cripple Creek district. Normalization values of Taylor and McLennan (1985). Also shown for comparison is a typical pattern for oceanic island basalt (OIB) from Wilson (1989).

fractional crystallization without contamination by upper crustal rocks was the dominant process. Oxygen isotope variations of about 2 per mil or more should be attributed to factors such as crustal contamination or subsolidus exchange (Taylor and Epstein, 1962a; Taylor and Sheppard, 1986). The difference in δ values between Cripple Creek phonotephrite and more felsic rocks in the suite (excluding trachyandesite) is 1.8 per mil (Table 3). Although small amounts of upper crustal contamination cannot be precluded, the relatively restricted range in values suggests that fractional crystallization was the dominant process, as was inferred from major and trace element data. Furthermore, the relatively low $\delta^{18}O$ values ($<9‰$) are consistent with a magma source in the upper mantle or lower crust (Taylor and Sheppard, 1986) and indicate that upper crustal contamination was not significant in the evolution of the Cripple Creek magmas.

Lead isotope geochemistry

Feldspar separates from least altered igneous rocks (Table 4) show a small compositional range in lead isotope composition (Fig. 10). Values for $^{206}Pb/^{204}Pb$, $^{207}Pb/^{204}Pb$, and $^{208}Pb/$

TABLE 3. Oxygen Isotope Compositions of Mineral Separates from Least Altered Igneous Rocks from the Cripple Creek District (values in per mil relative to SMOW; uncertainty ± 0.1‰)

Sample no.	Rock type	K feldspar	Plagioclase	Clinopyroxene	Magnetite	Magma[1]
CCPH1	Tph	7.2			2.8	8.2
CC009	Tph		7.1	6.0		8.1
CC007	Tta		7.4		2.3	8.4
CC010	Ttp	6.7		6.0		7.7
CC005	Tpt		7.5	5.8	6.0	7.1
CC008	Tpt		6.8	5.3	5.2	6.4
CCTM1	Tm				4.6	
CCTM1	Tm				4.9	

Tm = monchiquite, Tph = phonolite, Tpt = phonotephrite, Tta = trachyandesite, Ttp = tephriphonolite

[1] Magma compositions for phonolite, trachyandesite, and tephriphonolite were estimated based on a melt-feldspar fractionation of 1‰, similar to rhyolites (Taylor and Sheppard, 1986) and phonolites from the Laacher See volcanic field (Wörner et al., 1987); phonotephrite was assumed to have a negative melt-plagioclase fractionation of −0.4, similar to basalts (Taylor and Sheppard, 1986)

^{204}Pb range from 17.901 to 18.104, 15.508 to 15.532, and 38.354 to 38.558, respectively. Albite from trachyandesite is less radiogenic than the phonolitic rocks (^{206}Pb/^{204}Pb = 17.657, ^{207}Pb/^{204}Pb = 15.519, and ^{208}Pb/^{204}Pb = 38.156). On the uranium-derived lead diagram (^{207}Pb-^{206}Pb), the feldspars collectively plot below and to the left of expected average Tertiary compositions (essentially equal to present-day values, or at 0 on the Stacey-Kramer growth curve). This indicates that source rocks for Cripple Creek magmas maintained low U/Pb ratios for a significant period of geologic time. In contrast, the thorogenic lead ratios (^{208}Pb/^{204}Pb) are close to expected average Tertiary compositions, indicating that the source rocks had average Th/Pb ratios. The low U/Pb and average Th/Pb (i.e., high Th/U) ratios are consistent with material that has evolved in the lower crust after granulite metamorphism has preferentially expelled U relative to Th (Doe and Zartman, 1979).

The involvement of lower crust in the evolution of the Cripple Creek phonolites is illustrated qualitatively by comparing Cripple Creek lead isotope compositions to fields for midocean ridge basalts (MORB), within oceanic island basalts (OIB), and crustal rocks (Zartman and Doe, 1981, and Zartman and Haines, 1988; Fig. 10). A typical modern-day (essentially equivalent to 30 Ma) mantle-derived magma has present-day ^{206}Pb/^{204}Pb, ^{207}Pb/^{204}Pb, and ^{208}Pb/^{204}Pb values of 18.47, 15.48, and 37.73, respectively ("M"; Fig. 10), whereas lower crust has ^{206}Pb/^{204}Pb, ^{207}Pb/^{204}Pb, and ^{208}Pb/^{204}Pb ratios of 17.62, 15.35, and 38.75 ("LC"; Fig. 10). Tie lines drawn between these two reservoirs represent simple mixing lines, and mantle-derived magmas that have been contaminated by lower crustal rocks should lie on these lines. Cripple Creek rocks have compositions that lie along the lines between mantle and lower crust, at least with respect to ^{206}Pb/^{204}Pb and ^{208}Pb/^{204}Pb composition (Fig. 10). The higher ^{207}Pb/^{204}Pb ratios of Cripple Creek rocks compared to that predicted by the tie lines may indicate that the lower crustal component involved in the evolution of the Cripple Creek magmas had higher ^{207}Pb/^{204}Pb ratios compared to average values. This is supported by lead isotope compositions of gneiss (granulite) and amphibolite of the Idaho Springs Formation (1.8 Ga) from central Colorado (Stein, 1985); the ^{207}Pb/^{204}Pb ratios of these rocks, which range from 15.52 to 15.75, are higher than average lower crust.

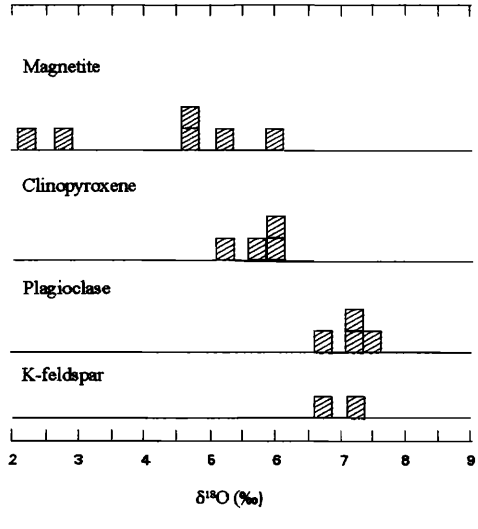

FIG. 9. Histograms illustrating the distribution of δ^{18}O values for feldspar, pyroxene, and magnetite from unaltered igneous rocks of the Cripple Creek district.

In contrast to the significant involvement of lower crustal rocks in the evolution of the Cripple Creek magmas, the data suggest there was little contamination from upper crustal rocks. The isotopic compositions of Cripple Creek feldspars are significantly less radiogenic than upper crustal rocks (Fig. 10).

Strontium isotope geochemistry

Eight whole-rock samples from the Cripple Creek district were collected by Birmingham (1987) for strontium isotope analyses (Table 5). The sample numbers of seven samples collected during this study that are compositionally equivalent to Birmingham's samples are shown in parenthesis in Table 5; five of these samples were collected from the exact sample locality as that used by Birmingham (1987). This was done so that geochemical and isotopic data obtained during this study could be used in conjunction with previously obtained data.

Initial ^{87}Sr/^{86}Sr ratios for the igneous rocks were calculated by Birmingham (1987) using an assumed age of 28.6 ± 4.9 Ma. The initial ^{87}Sr/^{86}Sr ratios were recalculated using ^{40}Ar/^{39}Ar ages obtained during this study (Table 5). A general distinction between phonolite and other rocks in the suite

TABLE 4. Lead Isotope Compositions of Feldspar from Least Altered Igneous Rocks in the Cripple Creek District

Unit	Sample no.	Mineral	$^{206}Pb/^{204}Pb$	$^{207}Pb/^{204}Pb$	$^{208}Pb/^{204}Pb$
Phonolite	CC004-K	K feldspar	17.901	15.512	38.486
Phonolite	CCPH1-K	K feldspar	17.975	15.522	38.407
Phonolite	CC009-K	K feldspar	17.931	15.521	38.535
Phonolite	CC009-P	Plagioclase	17.944	15.530	38.558
Trachyandesite	CC007-P	Plagioclase	17.657	15.519	38.156
Tephriphonolite	CC010-K	K feldspar	18.007	15.508	38.354
Tephriphonolite	530N2-P	Plagioclase	18.050	15.532	38.430
Phonotephrite	CC005-P	Plagioclase	18.104	15.532	38.509
Phonotephrite	CC008-P	Plagioclase	17.993	15.515	38.519

can be made on the basis of Rb and Sr contents and initial $^{87}Sr/^{86}Sr$ ratios. Rocks in the compositional range from monchiquite through tephriphonolite have Rb contents of ≤90 ppm, Sr contents of ≥1,700 ppm, Rb/Sr ratios of ≤0.05 (Table 2), and similar initial $^{87}Sr/^{86}Sr$ ratios that cluster from 0.70391 to 0.70474 (Table 5). Phonolite has relatively higher Rb (≥126 ppm) and lower Sr contents (≤1,300 ppm), yielding higher overall Rb/Sr ratios (≥0.1; Table 2) and a greater range of initial $^{87}Sr/^{86}Sr$ ratios (0.70431–0.71148). The highest initial ratio is from phonolite collected outside the complex (sample B-159), whereas phonolite collected within the complex (samples B-124 and B-120) yielded relatively lower ratios (Table 5).

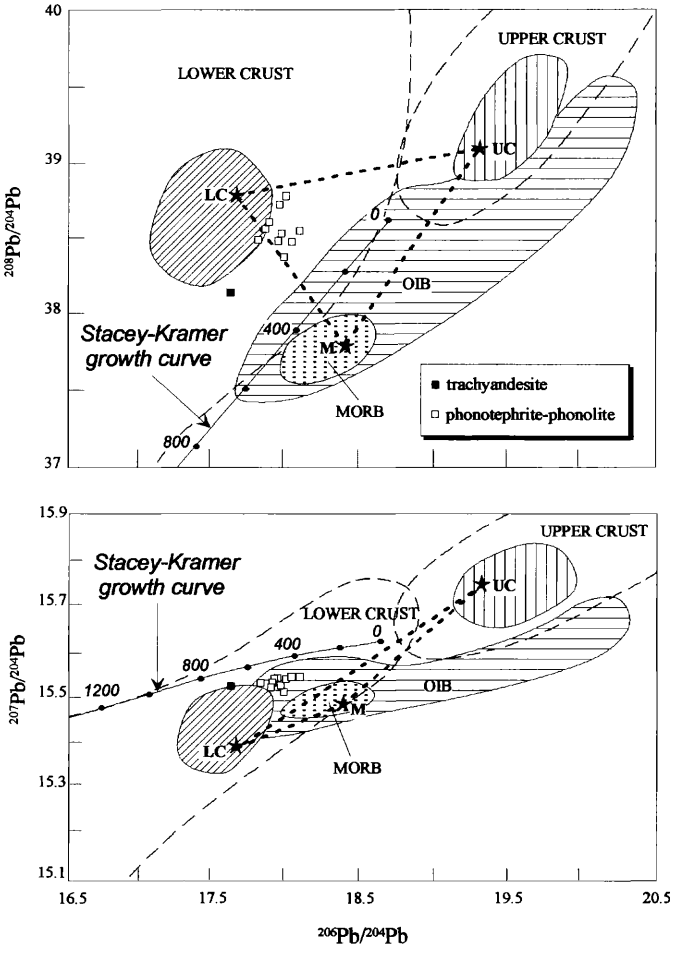

FIG. 10. Variation of $^{207}Pb/^{204}Pb$-$^{206}Pb/^{204}Pb$ and $^{208}Pb/^{204}Pb$-$^{206}Pb/^{204}Pb$ for Cripple Creek feldspars from igneous rocks compared to fields for mid-ocean ridge basalt (MORB), oceanic island basalt (OIB), and crustal rocks (from Zartman and Doe, 1981; Zartman and Haines, 1988). Solid lines enclose average values for each field and dashed lines enclose 80 percent of all data points for upper and lower crust. Also shown by stars are modern isotopic compositions (essentially equal to 30 Ma compositions) for mantle (M) and lower and upper crust (LC, UC; Zartman and Haines, 1988). Lines drawn between these end members represent simple mixing lines. See text for discussion.

The strontium isotope compositions of the relatively more mafic rocks in the suite (0.70391–0.70474) are consistent with a metasomatized mantle source for these magmas (i.e., $^{87}Sr/^{86}Sr_i$ of subcontinental lithospheric mantle = 0.7035–0.7100; observed range in oceanic island basalts = 0.7028–0.7070; McDonough et al., 1985). However, the more radiogenic ratios of the phonolites suggest that these magmas may have been contaminated by assimilation of enriched radiogenic upper crustal material. This contrasts with previous discussions of the lead and oxygen isotope data which indicated minimal upper crustal contamination. It is possible that the low Sr contents and high initial Sr ratios of phonolite without associated increases in $^{206}Pb/^{204}Pb$ or $\delta^{18}O$ may be a result of postcrystallization hydrothermal alteration (lead and oxygen analyses were performed on relatively fresh mineral separates, whereas whole-rock samples were used for strontium isotope analyses). However, the phonolite with the highest strontium ratio was collected outside the complex, and in general, these rocks are the least altered rocks (Birmingham, 1987; Kelley, 1996). Alternatively, the high Sr ra-

TABLE 5. Strontium Isotope Compositions of Whole-Rock Samples from the Cripple Creek District

Unit	Sample no.[1]	$^{87}Sr/^{86}Sr_i^a$	$^{87}Sr/^{86}Sr_i^{\sim}$
Phonolite	B-159 (CCPH1)	0.71249	0.71148
Phonolite	B-124 (CC004)	0.70600	0.70600
Phonolite	B-128 (CC009)	0.70431	0.70474
Phonolite	B-120	0.70475	0.70431
Tephriphonolite	B-165 (CC010)	0.70391	0.70391
Phonotephrite	B-127 (CC008)	0.70433	0.70433
Phonotephrite	B-130 (CC005)	0.70434	0.70434
Lamprophyre	B-150 (CCTM1)	0.70460	0.70460

[1] Sample number in parenthesis refers to sample from this study that is equivalent in composition to that collected by Birmingham (1987); some of these samples (CC005, CC008, CC009, CC010, and CCTM1) were collected from the same location as that collected by Birmingham (1987)

a = values from Birmingham (1987); i = initial ratios which were calculated using an assumed age of 28.6 ± 4.9 Ma; ~ = the age corrected initial ratios reported here were calculated using $^{40}Ar/^{39}Ar$ ages obtained in this study

tios of phonolite without increases in lead or oxygen compositions may be attributed partly to the contrast in isotopic composition between the contaminant (upper crustal rocks) and the magmas. For instance, upper crustal rocks typically have average Sr concentrations of about 350 ppm and initial ratios of 0.7149 (Zartman and Haines, 1988). The low Sr content of Cripple Creek phonolite (as low as 18 ppm) makes them much more easily contaminated by upper crustal-derived radiogenic ^{87}Sr than the other magmas, and therefore, much more sensitive indicators of upper crustal contamination. However, the lead compositions of the contaminant (upper crust) and Cripple Creek magmas are not significantly different (i.e., Pb is 11–50 ppm in Cripple Creek magmas and 20–25 ppm in upper crustal rocks; Zartman and Haines, 1988). This may result in Sr isotope compositions that are strongly affected by small amounts of contamination by upper crustal rocks, without increases in lead isotope compositions.

The amount of contamination may be qualitatively assessed by the difference in initial ratios between phonolite collected within the complex (0.70474 and 0.70600) and the high ratio of phonolite outside of the complex (0.71148). Magmas intruded into the complex may have ascended relatively rapidly without extreme interaction with crustal rocks. Conversely, phonolite outside the complex may have had difficulty ascending through granitic basement rocks and therefore had a greater degree of crustal interaction.

Geochronology

Previous age relationships of rocks within the Cripple Creek complex were based primarily on relative ages as determined from crosscutting field relationships and on ages of the phonolite and syenite (tephriphonolite) that were obtained by conventional K-Ar analyses. Wobus et al. (1976) obtained dates for phonolite of 27.9 ± 0.7 and 29.3 ± 0.7 Ma based on two samples; however, the locations and nature of the samples (whole rocks or mineral separates) were not specified. In addition, McDowell (1971) determined dates of 33.4 ± 1.0 and 33.8 ± 1.3 Ma for aegerine-augite from syenite collected from a mine dump in the east-central part of the complex.

In order to determine more precise ages for the igneous rocks and mineralized samples, $^{40}Ar/^{39}Ar$ dating methods were used. The minerals selected for analysis were either K feldspar (sanidine or adularia) or biotite; whole-rock samples were used in cases where K-bearing minerals were either absent or present in only trace amounts.

$^{40}Ar/^{39}Ar$ age spectra

Seven of the 13 samples analyzed yielded plateau ages (Table 6; Figs. 11 and 12), which are defined as the part of the release spectrum in which contiguous gas fractions have similar ages and comprise more than 50 percent of the total ^{39}Ar released (Fleck et al., 1977). Ages are considered to be similar if no difference can be detected at the 95 percent level of confidence, using the critical value test of Dalrymple and Lanphere (1969). The error calculated for the plateau age is the standard deviation of the ages of all fractions on the plateau.

If no age plateau is present, the sample is considered disturbed. Many of the samples that did not yield plateau ages have spectra that form saddle-shaped patterns, with a minimum in the central or high-temperature part of the release (e.g., sample CC009; Fig. 11e or sample CC001B, Fig. 12g). Such saddle-shaped spectra are diagnostic of the presence of excess ^{40}Ar (Lanphere and Dalrymple, 1976). However, some of these spectra exhibit flat plateaulike segments, and ages were calculated, with weighting for the size of steps (average weighted mean ages; Table 6). In addition, isotope diagrams ($^{40}Ar/^{36}Ar$ vs. $^{39}Ar/^{36}Ar$) were constructed and isochron ages were calculated for samples not yielding plateau ages (Fig. 13). The measured $^{40}Ar/^{36}Ar$ and $^{39}Ar/^{36}Ar$ ratios of incremental gas fractions define a series of points that may fit a straight line, or isochron, whose slope is the $^{40}Ar_R/^{39}Ar$ ratio that is related to the age of the sample (York, 1969). The intercept of the isochron is the $^{40}Ar/^{36}Ar$ ratio of the trapped argon or nonradiogenic fraction of the gas associated with a given sample. If the intercept is greater than 295.5 (the atmospheric $^{40}Ar/^{36}Ar$ ratio as recommended by Steiger and Jäger, 1977), the sample has excess ^{40}Ar; if it is less than 295.5, the sample has experienced radiogenic argon loss.

In constructing the isotope diagrams, only selected steps were used. Generally, those steps that did not show excess argon in the spectra (usually the intermediate temperature steps), those that gave greater than 80 percent radiogenic yields, and those having consistent $^{39}Ar/^{37}Ar$ ratios were used. The $^{39}Ar/^{37}Ar$ ratio is approximately equivalent to the K/Ca ratio, which reflects the composition of the mineral degassed.

Early igneous activity: The earliest igneous activity is represented by $^{40}Ar/^{39}Ar$ ages of 32.5 ± 0.1 to 30.9 ± 0.1 (1σ) Ma for relatively felsic phonolitic rocks. These include from oldest to youngest, tephriphonolite, phonolite, trachyandesite, and a second episode of phonolite (Table 6). Sanidine from tephriphonolite (sample 89CC010S; App.) yielded a well-behaved spectrum and a plateau age of 32.5 ± 0.1 Ma on three steps that contain 55 percent of the total ^{39}Ar released (Fig. 11a). Similarly, the spectrum of biotite from the N2 tephriphonolite dike shows that the intermediate- and high-temperature steps (800–1,300°C) form a plateau (93% of the total gas released) with a date of 32.3 ± 0.1 Ma (Fig. 11b), which is statistically identical to the sanidine plateau age from sample CC010.

Phonolite samples yielded ages of 31.8 to 30.9 Ma. The spectrum for sanidine sample CCPH1 (Fig. 11c) contains a plateau, defined by five contiguous steps representing 64 percent of the gas released, with an apparent age of 30.9 ± 0.1 Ma (800°–1,100°C). Sanidine from sample 89CC004 (Fig. 11d) is characterized by low-temperature steps (constituting about 7% of the total $^{39}Ar_K$ released), with anomalously old apparent ages which suggests the presence of excess argon in the sample. Intermediate- to high-temperature steps (1,100°–1,200°C) produce a relatively flat segment of the spectra; however, these steps represent only 32 percent of the total $^{39}Ar_K$ released, and, therefore, do not define a plateau as defined above. Therefore, an average weighted mean age of 31.8 ± 0.2 Ma was calculated. This is believed to be the best estimate of the age of sample CC004 due to the good radiogenic yields (>95%) and internally consistent K/Ca ($^{39}Ar/^{37}Ar$) ratios of >10 (App.), reflecting a consistent mineral composition over this temperature interval.

Sanidine from sample CC009 (phonolite) yielded a complex saddle-shaped age spectrum (Fig. 11e) with apparent ages of low- and high-temperature steps exceeding 50 Ma,

TABLE 6. Summary of $^{40}Ar/^{39}Ar$ Age Spectrum Data for Rocks and Mineralized Samples from the Cripple Creek District (number refers to sample localities shown in Figure 2)

Number	Sample no.	Rock type	Sample type[1]	Plateau age Ma ± 1σ	Average weighted mean age	Isochron age Ma ± 1σ	Preferred age Ma ± 1σ
Early igneous activity							
1	CC010S	Tephriphonolite	sa	32.5 ± 0.1			32.5 ± 0.1
2	530N2	Tephriphonolite	bi	32.3 ± 0.1			32.3 ± 0.1
3	CC004	Phonolite	sa		31.8 ± 0.2		31.8 ± 0.2
4	CC009	Phonolite	sa		31.6 ± 0.2	31.9 ± 0.2	31.6[2]
5	CC007	Trachyandesite	wr			31.6 ± 0.2	31.5[2]
6	CCPH1	Phonolite	sa	30.9 ± 0.1			30.9 ± 0.1
Late igneous and hydrothermal activity							
7	CC003	Adularia-biotite-pyrite vein	ad	31.3 ± 0.1			31.3 ± 0.1
8	37K122	Biotite-pyrite-quartz vein	bi	29.9 ± 0.1			29.9 ± 0.1
9	CRESA-4	Matrix of breccia with disseminated native gold and pyrite	ad	29.8 ± 0.1			29.8 ± 0.1
10	CC2	Adularia-quartz vein	ad	29.6 ± 0.1			29.6 ± 0.1
11	CC005	Phonotephrite (Isabella dike)	wr			29.1 ± 0.2	28.7[2]
12	CC001A	Altered phonolite	sa-ad			28.8 ± 0.1	28.8 ± 0.1
13	CC001B	Altered phonolite	ad			28.2 ± 0.1	28.2 ± 0.1

[1] ad = adularia, bi = biotite, sa = sanidine, wr = whole rock

[2] This age is derived from the minimum age in the spectrum, and because of excess ^{40}Ar, it is taken to represent the maximum age for this sample; the true age is any age less than this maximum indicated age

which are clearly geologically unreasonable. The K/Ca ratios for these low- and high-temperature intervals are relatively low compared with other parts of the spectrum and indicate that some mineral other than sanidine degassed. Plagioclase or low K feldspathoid minerals intergrown with sanidine are the most likely impurities (Kelley, 1996). There is a flattening of the spectrum at 800° to 850°C, with an average weighted mean age of 31.6 ± 0.2 Ma (represented by 20% of the gas released), which is in close agreement with the calculated isochron age (Table 6). The gas produced at these temperatures contains relatively more consistent and higher K/Ca ratios, indicating that sanidine was probably the mineral-contributing gas over this interval. Based on this information, the age of sample CC009 is interpreted to be the average weighted mean age of 31.6 ± 0.2 Ma. However, the calculated initial $^{40}Ar/^{36}Ar$ ratio of 460 ± 8.7 for these two temperature steps clearly indicates the presence of excess argon, and therefore, the interpreted age of 31.6 Ma is considered a maximum age for this sample. The true age of the sample could be any age younger than 31.6 Ma.

Similar to most phonolite samples, the age spectrum for trachyandesite (whole rock) is characterized by excess argon at low temperatures, yielding anomalously old apparent ages (Fig. 11f). Although no plateau was defined, there is a general stepping down of the spectrum at intermediate- and high-temperature steps (1,100°–1,400°C). Gas fractions released over this temperature interval represent 79 percent of the total $^{39}Ar_K$ released and are characterized by consistent K/Ca ratios and good radiogenic yields (>89%). The calculated isochron age of 31.6 ± 0.2 Ma is considered a maximum age because $^{40}Ar/^{36}Ar$ ratios greater than atmospheric values suggest the presence of excess argon (Fig. 13). Therefore, the minimum age reflected in the spectrum (31.5 Ma) is chosen as representing the maximum age of the trachyandesite (Table 6).

In summary, the earliest igneous activity included emplacement of tephriphonolite, phonolite, and trachyandesite within the complex over at least 1 m.y., from 32.5 to 31.5 Ma. A younger episode of phonolite emplacement is indicated by an age of 30.9 ± 0.1 Ma for sample CCPH1 collected 6 km east and outside of the complex.

Late igneous and hydrothermal activity: Based on crosscutting relationships, Loughlin and Koschmann (1935) suggested that the earliest veins in the district (quartz-K feldspar-biotite-fluorite-dolomite-pyrite) may have formed during or after emplacement of phonolite, followed by emplacement of mafic and ultramafic rocks (phonotephrite and lamprophyre), and then by formation of the most productive Au-Te vein deposits (Loughlin and Koschmann, 1935). Field relationships also suggest that there was most likely at least one more episode of lamprophyre dike emplacement that postdated all other rocks in the district, including the Au-Te veins (Loughlin and Koshmann, 1935; Thompson et al., 1985; Pontius, 1996). In general, this simplified sequence of events is relatively consistent throughout the district, but ages obtained during this study and recent work by Jensen and Barton (1997) suggest that the magmatic and hydrothermal history may have been more complex. For instance, as stated in the previous section, there were two rather than one stage of phonolite emplacement. In addition, although there are some quartz-K feldspar-biotite-fluorite-dolomite-pyrite veins that clearly predate mafic and ultramafic rocks, there are others which postdate them (Eric Jensen, writ. commun., 1998).

Perhaps the most consistent and well-documented relationship is the emplacement of phonotephrite and lamprophyre dikes prior to formation of the Au-Te veins. These crosscutting relationships are observed in many places in the district. For instance, in the Goldstar pit, the Isabella phonotephrite dike is cut by the northeast-trending Pharmacist vein, which consists primarily of tellurides and quartz and was one

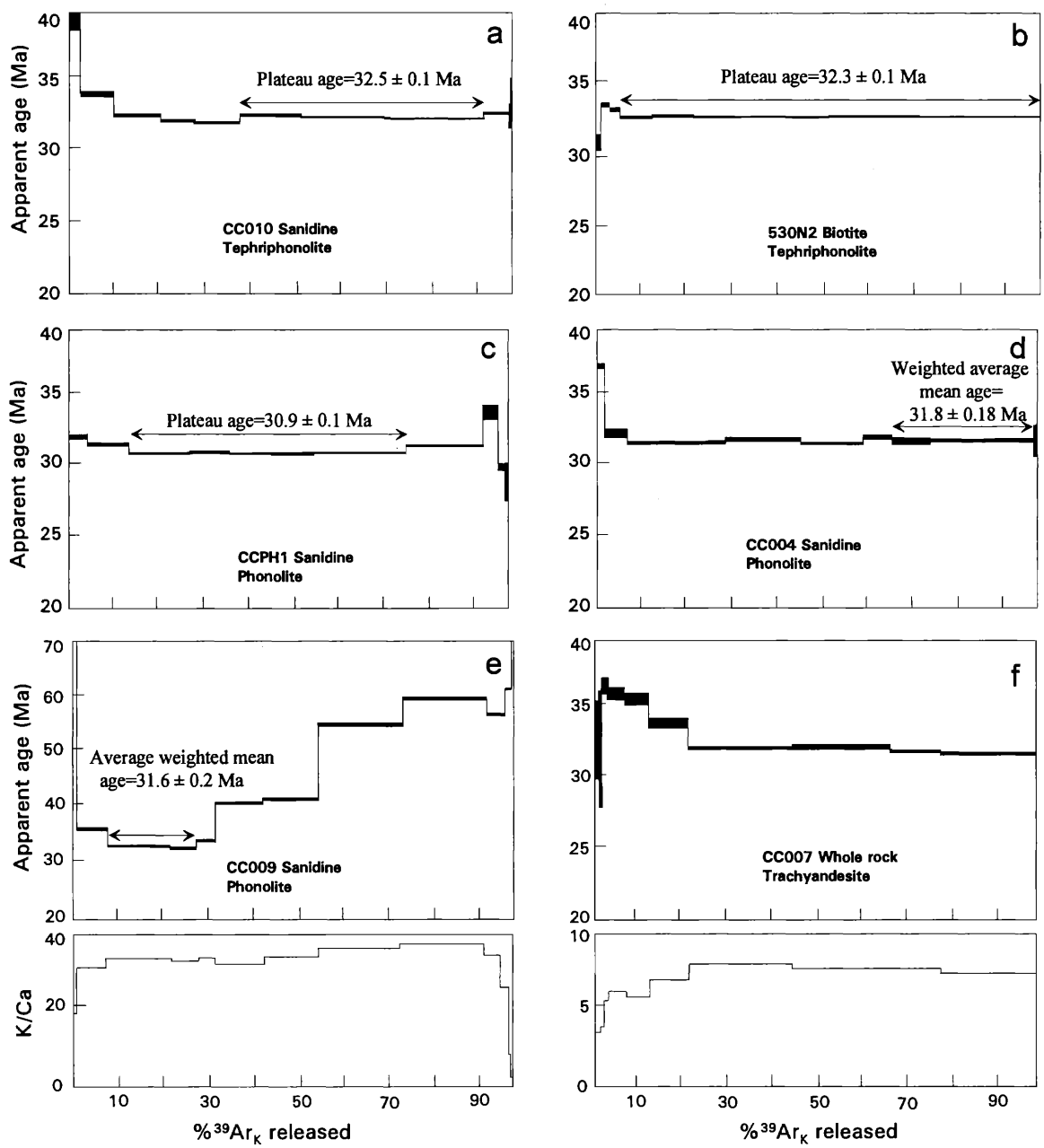

FIG. 11. $^{40}Ar/^{39}Ar$ age spectrum diagrams for tephriphonolite, phonolite, and trachyandesite, which represent the early igneous activity at Cripple Creek. The K/Ca ($^{39}Ar/^{37}Ar$) ratios are shown for samples not yielding plateau ages.

of the most productive gold-telluride veins in the district (Lindgren and Ransome, 1906). Similarly, the Cresson pipe, which is composed of fragments of lamprophyric rocks set in a matrix of lamprophyre and fine-grained fragmental material, contains high-grade gold telluride minerals that were deposited after pipe formation as open-space fillings (Loughlin and Koschmann, 1935). These relationships clearly illustrate that the timing of mafic and ultramafic dike emplacement is critical for constraining the age of Au-Te mineralization.

Also important for understanding the timing of gold mineralization in the district is the temporal and genetic relationship between the vein and disseminated gold-pyrite styles of mineralization. Pontius (1996) suggested that the disseminated mineralization probably formed as an upper level and (or) lateral expression of the high-grade Au-Te systems. Crosscutting relationships between the two styles of mineralization have not been well established. However, it is clear that relatively higher grade gold in the disseminated deposits is associated with pervasive K feldspar alteration zones (Pontius, 1996), and that native gold is, in places, encapsulated within adularia in these deposits, suggesting that adularia was contemporaneous with gold mineralization (Eric Jensen, writ. commun., 1998). Furthermore, the pervasive K feldspar alteration zones associated with disseminated gold cut across early igneous rocks (tephriphonolite and phonolite), as well as phonotephrite and lamprophyre (Eric Jensen, writ. commun.,

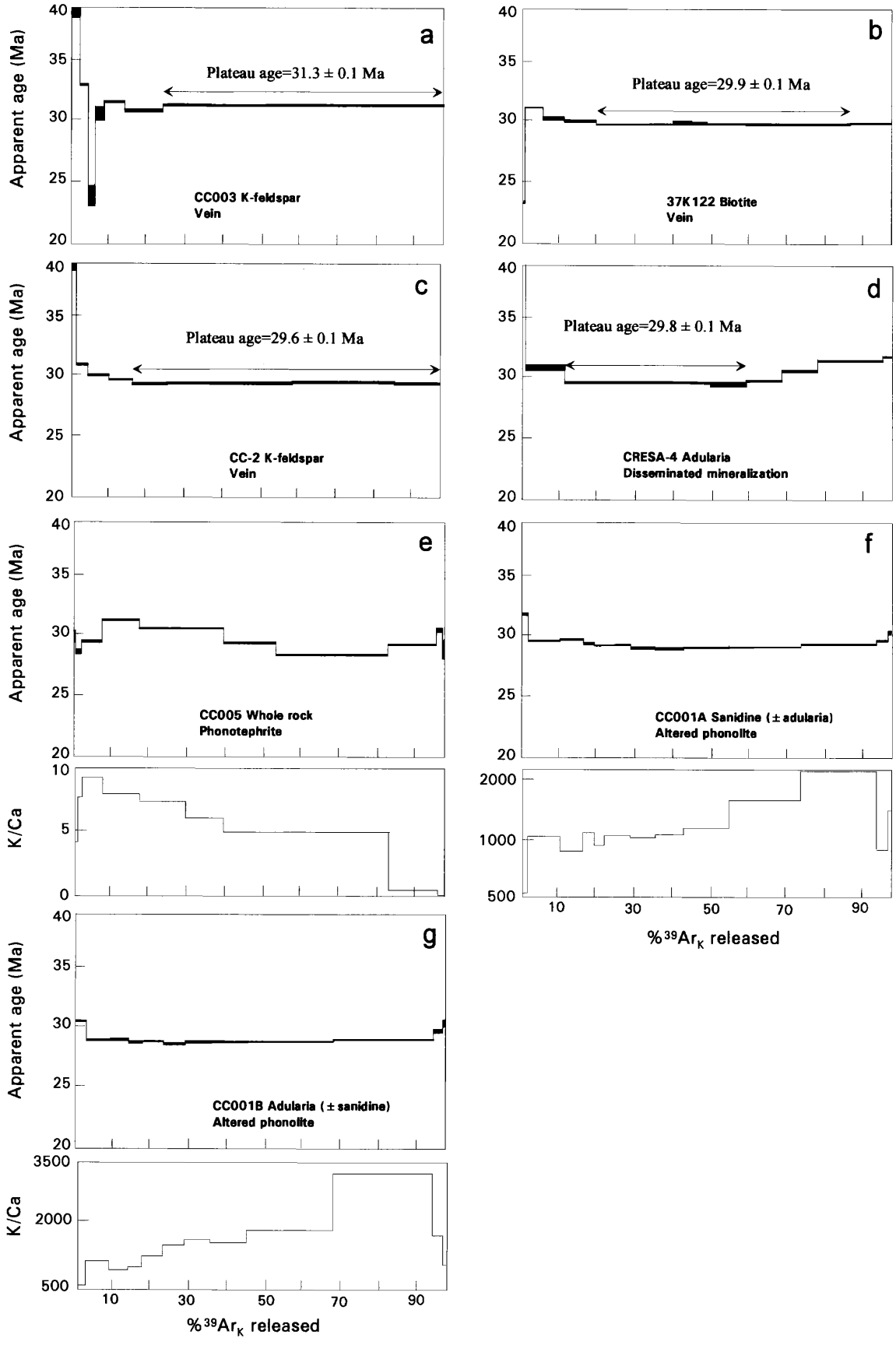

FIG. 12. $^{40}Ar/^{39}Ar$ age spectrum diagrams for adularia and biotite from vein and disseminated mineralized zones, K feldspar from altered phonolite, and phonotephrites which represent late magmatic activity.

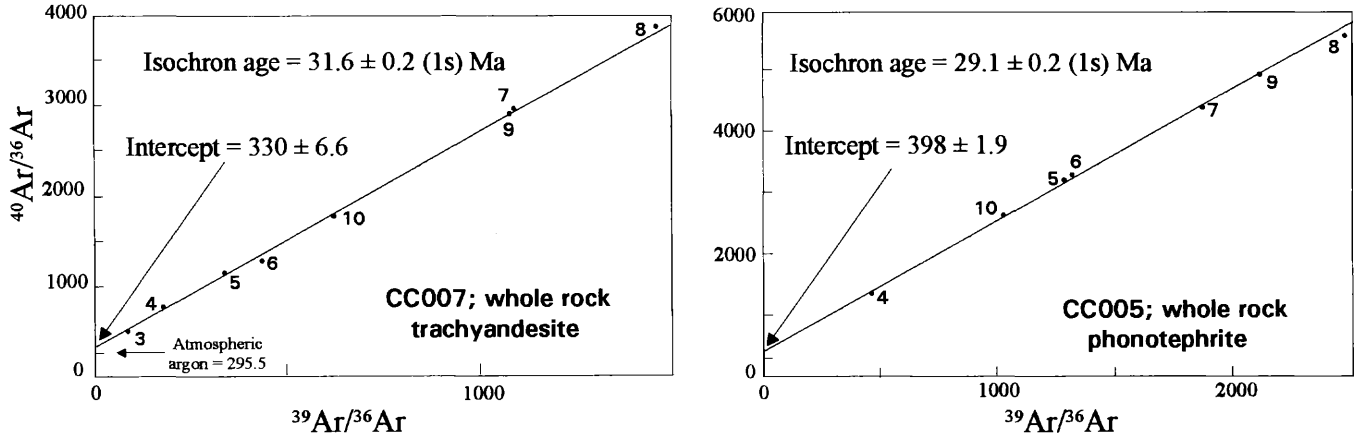

FIG. 13. $^{40}Ar/^{36}Ar$ vs. $^{39}Ar/^{36}Ar$ isotope correlation diagrams for whole-rock samples listed in Table 6. Lines represent linear regressions of data. Numbers next to points refer to select temperature steps.

1998). This suggests that the disseminated gold, as is the case for the Au-Te veins, formed after mafic and ultramafic dike emplacement.

Given the absence of suitable minerals for direct dating of the gold-forming event, placing constraints on the timing of gold mineralization at Cripple Creek is dependent on obtaining ages for biotite or K feldspar from veins and alteration zones associated with disseminated gold, as well as phonotephrite and lamprophyre. All of the vein samples analyzed during this study yielded well-behaved plateau ages (31.3 ± 0.1–29.6 ± 0.1 Ma; Table 6; Fig. 12) that place an upper age constraint on the gold-forming event because paragenetic studies indicate that K feldspar and biotite preceded deposition of gold tellurides in the veins (Lindgren and Ransome, 1906; Thompson et al., 1985). Sample 89CC003, a K feldspar separate from a biotite-K feldspar-pyrite vein, yielded a spectrum which is characterized by excess argon at low-temperature intervals, followed by a relatively flat age spectrum at intermediate- to high-temperature steps (Fig 12a). The plateau age of 31.3 ± 0.1 Ma is defined by three contiguous steps containing 76 percent of the gas released. The spectrum for sample 37K122 (biotite) contains a plateau defined by six contiguous steps, representing 69 percent of the gas released, with an apparent age of 29.9 ± 0.1 Ma (850°–1,150°C; Fig. 12b). A plateau age of 29.6 ± 0.1 Ma for vein K feldspar from the Goldstar open-pit mine (CC-2; Fig. 12c) was obtained for the 900° to 1,450°C temperature steps and includes 83 percent of the total gas released.

Fine-grained adularia from the matrix of a breccia (Fig. 3E) containing disseminated pyrite and gold in the Cresson deposit (sample CRESA-4; Fig. 12d) yielded a plateau age of 29.8 ± 0.1 Ma, which is statistically similar to (i.e., apparent ages overlap within analytical error) the 29.6 ± 0.1 Ma age yielded by vein K feldspar. Two additional ages were obtained for potassically altered phonolite adjacent to the Pharmacist vein in the Goldstar pit. Field relationships indicate that the Pharmacist vein and this pervasive zone of potassic alteration cut the Isabella dike. A coarse fraction (−60, +100 mesh) was obtained to represent primarily phenocryst sanidine (CC001A; Fig. 12f), and a fine fraction (−120, +140 mesh) was separated, which represents primarily K feldspar-flooded matrix material (CC001B; Fig. 12g). Both fractions yielded similar age spectra, characterized by excess argon at low temperature followed by a drop in ages and flattening of the spectra. Calculated isochron ages are 28.8 ± 0.1 and 28.2 ± 0.1 Ma, respectively (Table 6). The $^{40}Ar/^{36}Ar$ ratios were only slightly greater than atmospheric values, indicating only minor excess argon. For this reason, the 28.8 ± 0.1 and 28.2 ± 0.1 Ma are the preferred ages for these two samples (Table 6).

To place further constraints on the timing of gold mineralization, four samples of phonotephrite and lamprophyre were analyzed using the $^{40}Ar/^{39}Ar$ method. Unfortunately, due to extreme excess argon, the age spectra for three of these samples (whole rock and biotite) were uninterpretable (Kelley, 1996). However, a date was obtained for a whole-rock sample of phonotephrite from the Isabella dike in the Goldstar pit (CC005; Fig. 12e). The spectrum is characterized by a series of gradually decreasing apparent ages of 29.6 to 28.7 Ma from 800° to 1,200°C, with no well-defined plateau. Over this temperature interval, the radiogenic yields were greater than 90 percent and K/Ca ratios were relatively consistent (Fig. 12e). Isochron regression yielded an age of 29.1 ± 0.2 Ma, but the initial $^{40}Ar/^{36}Ar$ ratio of 398 ± 1.9 (1σ) suggests this temperature interval includes excess ^{40}Ar (Fig. 13). The interpreted age for sample CC005 is between 28.7 and 29.1 Ma (the age yielded by isochron regression), but due to the presence of excess ^{40}Ar, it is most likely closer to the relatively younger age of 28.7 Ma (Table 6). Furthermore, due to the presence of excess ^{40}Ar, this age (28.7 Ma) represents a maximum age for this sample.

Although it is tempting to conclude from these data that mafic phonotephrite was emplaced at least 2 m.y. after the relatively more felsic rocks, it is unwarranted based on a single age. This is particularly true due to uncertainties in the interpretation of the age spectrum from sample CC005 because it is a whole rock rather than a pure mineral separate, and therefore, it consists of a number of phases of different argon retentivity. Furthermore, if the interpreted age for this sample is close to the true age of the phonotephrite, it is difficult to integrate with the observed field relationships or previously described age data, especially if it is assumed that, district-wide, there was one mafic-ultramafic igneous event followed by a single mineralizing event. For instance, if it is

assumed that the main gold-forming event began at about 29.8 (age of adularia from the Cresson disseminated deposit) to 29.6 Ma (upper age limit for gold mineralization set by paragenetically early vein minerals), then the age for the mafic and ultramafic rocks would necessarily have to be older than 29.8 Ma, not less than 28.7 Ma, as suggested by the Isabella dike sample.

However, the data are easily explained if it is assumed that there may have been more than one episode of mafic-ultramafic igneous rock emplacement. For instance, during the waning stages of phonolite emplacement at about 30 to 31 Ma, an early episode of mafic-ultramafic intrusion may have occurred, which was closely followed by deposition of biotite and K feldspar and then Au-bearing minerals in veins throughout a large vertical extent and as disseminated zones at relatively shallower levels. The ages obtained for disseminated K feldspar from the Goldstar pit indicate that this hydrothermal activity may have continued, perhaps intermittently, for at least 2 m.y. It is not unreasonable to assume that, over this 2 m.y. period, there was one or more additional episodes of mafic and ultramafic dike emplacement.

Summary of age data

The timing of the development of the complex and the relative temporal relationships between alkaline igneous rocks and spatially related mineral deposits are known in part by field relationships and are further defined by the $^{40}Ar/^{39}Ar$ isotope ages (Fig. 14). Field relationships suggest that volcanic eruption, diatreme development, intrusion, and volcaniclastic and lacustrine sedimentation occurred throughout the evolution of the complex. The absolute age of the initial eruptive volcanism which produced tuffs and breccias of unit Tbr is uncertain but constrained by field relationships; rocks of unit Tbr overlie the Tallahassee Creek Conglomerate (Tw) northwest of the complex (Fig. 2). The Tallahassee Creek Conglomerate contains clasts of Wall Mountain Tuff (35–36.6 Ma; Epis and Chapin, 1975; Mertzman et al., 1994). Therefore, the upper age limit for unit Tbr is 35 Ma (Fig. 14). Additionally, the presence of Thirtynine Mile Andesite (34 Ma; Epis and Chapin, 1975) which underlies phonolite southwest of the complex places an upper age limit of 34 Ma for emplacement of phonolite flows, dikes, and plugs.

The $^{40}Ar/^{39}Ar$ ages suggest a complex magmatic and hydrothermal history. Tephriphonolite, trachyandesite, and phonolite were emplaced into the complex over about 1 m.y., from 32.5 ± 0.1 to 31.5 ± 0.1 Ma (Fig. 14) with a younger episode (30.9 ± 0.1 Ma) of phonolite outside of the complex. Field relationships suggest that mafic and ultramafic rocks were emplaced after the felsic phonolites and prior to the main gold mineralizing event. Constraints on the timing of mineralization are provided by paragenetically early vein minerals and adularia from the disseminated deposits. Early vein minerals (31.3 ± 0.1–29.6 ± 0.1 Ma) and adularia (29.8 ± 0.1 Ma) from the Cresson disseminated deposit formed concurrently (Fig. 14) and place upper age constraints on gold mineralization because K feldspar predates gold in veins, and adularia was probably concurrent with gold in the disseminated deposits. Two additional ages (28.8 ± 0.1 and 28.2 ± 0.1 Ma) for potassically altered phonolite adjacent to the Pharmacist vein suggest that there was a protracted hydrothermal history that continued, perhaps intermittently, for at least 2 m.y.

The absolute timing of the mafic-ultramafic igneous event

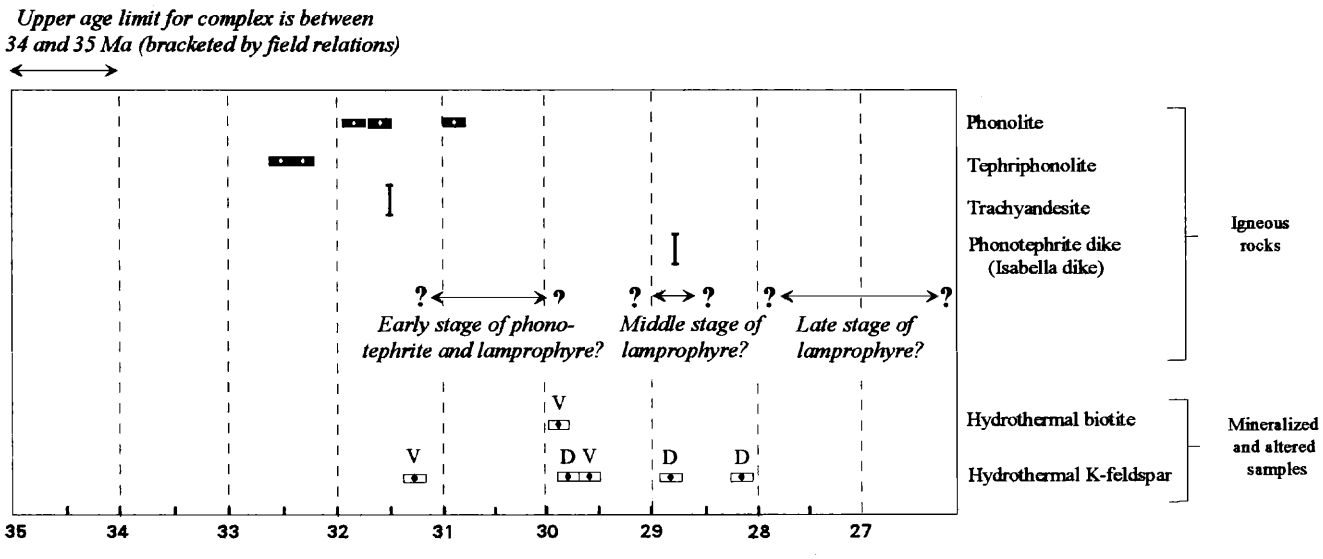

FIG. 14. Summay of ages for igneous rocks and mineralized vein samples from the Cripple Creek district. D = disseminated adularia-pyrite (± native Au) mineralization, V = vein-type mineralization.. Horizontal bar indicates age with associated error. Vertical bar indicates maximum age for sample of whole rock (see text for discussion). Field evidence suggests that mafic phonolite and lamprophyre postdate emplacement of felsic phonolitic rocks. A single whole-rock sample suggests this may have been at about 28.7 Ma or younger. Alternatively, or in addition to, field evidence suggests there was an event which preceded the main hydrothermal phase. Field relationships also suggest that there was a stage of lamprophyre dikes which postdated hydrothermal mineralization.

is not clear based on $^{40}Ar/^{39}Ar$ ages because reliable dates (i.e., plateau ages) were not obtained for these rocks. A single whole-rock sample of the Isabella dike (phonotephrite) yielded a maximum age of 28.7 Ma (i.e., the sample is younger than 28.7 Ma). However, if the interpreted age for this sample is close to the true age of the phonotephrite, it is difficult to integrate with the observed field relationships or previously described age data, which would suggest that mafic and ultramafic rocks were necessarily emplaced prior to 29.8 Ma (the assumed age of gold mineralization in the disseminated deposits). These discrepancies might be explained if more than one episode of mafic-ultramafic rock emplacement had occurred (Fig. 14). Additional ages from mafic and ultramafic rocks are needed to constrain more closely the timing of this later igneous event.

Relationship between Magmatism and Mineralization

Lead isotope data for K feldspar and galenas from vein and disseminated deposits

Lead isotopes provide a means of testing the proposed genetic relationship between the intrusive rocks and deposits at Cripple Creek, because they provide information about the source for the lead in a hydrothermal system. One sample of K feldspar and 19 samples of galena were collected from veins (Fig. 2). Four galena samples are from veins hosted by Precambrian wall rocks near the margins or outside of the Cripple Creek complex. The other galenas and the K feldspar sample are from veins hosted by Tertiary breccias and igneous rocks. Analytical results and a description of location and host-rock age are listed in Table 7.

Vein galena and K feldspar are either isotopically equal to or more radiogenic than the phonolitic rocks (Fig. 15). Except for three galena samples with $^{206}Pb/^{204}Pb$ values >18.34, the range in $^{206}Pb/^{204}Pb$ ratios of the K feldspar and galenas overlaps those of the phonotephrite-phonolite series. Furthermore, K feldspar from potassically altered phonolite coincident with gold mineralization in the Goldstar pit is isotopically indistinguishable from unaltered phonolite (Fig. 15; Table 7).

Although the $^{206}Pb/^{204}Pb$ ratios of most galenas are in close agreement with those of the phonolitic rocks, there is a distinct trend toward higher $^{207}Pb/^{204}Pb$ and $^{208}Pb/^{204}Pb$ ratios for some galenas relative to phonolitic rocks. This is particularly evident in the thorogenic lead isotope ratios (Fig. 15) and suggests a lead contribution to the ore fluids from Proterozoic rocks. Most of the galenas with the highest $^{207}Pb/^{204}Pb$ and $^{208}Pb/^{204}Pb$ compositions are from the margins or outside the complex (Fig. 15), and most, but not all, of these are hosted by Proterozoic rocks (Table 7). The general increase in $^{207}Pb/^{204}Pb$ and $^{208}Pb/^{204}Pb$ composition of galenas from the margin or outside the complex reflects the greater degree of interaction of ore fluids with Proterozoic rocks near the margins compared to the center of the complex where Tertiary rocks occur in greater thicknesses.

The contribution of lead to the ore fluid by leaching of Proterozoic rocks can be assessed in more detail by examination of the lead isotope compositions of unaltered Proterozoic rocks from central Colorado (Doe, 1970; Stein, 1985). Because the addition of radiogenic lead to the ore fluids from Proterozoic rocks is particularly evident in the thorogenic lead isotope ratios (Fig. 15), it might be concluded that Silver Plume Granite (part of the same intrusive suite as the Cripple Creek Quartz Monzonite), which has very high $^{208}Pb/^{204}Pb$ compositions (47.05–53.41; Stein, 1985), was the primary contaminant. However, the $^{206}Pb/^{204}Pb$ and $^{207}Pb/^{204}Pb$ ratios of Silver Plume Granite (17.35–18.00 and 15.49–15.55, respectively) are equivalent to or less radiogenic than most Cripple Creek galenas or phonolitic rocks. Therefore, leaching of lead from the Cripple Creek Quartz Monzonite by the

TABLE 7. Lead Isotope Compositions of Galenas and K Feldspar from Veins in the Cripple Creek District

Sample no[1]	$^{206}Pb/^{204}Pb$	$^{207}Pb/^{204}Pb$	$^{208}Pb/^{204}Pb$	Age of host rock[2]	Mine name	General location[3]
41-K-115-G	18.025	15.570	39.156	T	Index	NM
36-K-29-G	17.955	15.541	38.560	T	Moon Anchor	NM
31-K-163-G	18.158	15.540	38.963	PC	Conundrum	NM
31-K-118A-G	18.090	15.554	38.593	T	Mollie Kathleen	NM
31-K-118B-G	18.073	15.527	38.510	T	Mollie Kathleen	NM
31-K-149-G	18.157	15.551	39.012	T	Copper Mtn	OC
36-K-195-G	17.823	15.519	38.557	T	Orpha May	C
31-K-G	18.159	15.548	38.998	T	Copper Mtn	OC
89-AJ-BT-G	18.461	15.578	38.816	PC	Ajax	NM
89-AJ-NM-G	18.137	15.557	38.817	PC	Ajax	NM
25-L-86-G	17.892	15.518	38.310	T	American Eagle	C
36-L-5-G	17.995	15.536	38.458	T	Rose Nichol	SC
25-L-77-G	18.016	15.558	38.516	T	Dexter	SC
25-L-107-G	18.395	15.580	38.944	T	American Eagle	C
37-OT-G	17.917	15.533	38.335	T?	Ophelia Tunnel	OC
41-K-116-G	18.340	15.597	39.479	T	Index	NM
41-K-38-G	17.947	15.561	38.523	T	Proper	NM
41-K-39-G	17.914	15.519	38.382	T	Proper	NM
10-A-1-G	18.151	15.567	38.836	PC	Ajax	NM
89CC003-KV	18.043	15.551	38.759	T	Ocean Wave	SC
89CC001A-KD	18.010	15.528	38.769	T	Goldstar	C
89CC001B-KD	17.976	15.525	38.711	T	Goldstar	C

[1] Letter ending field number designates type of samples analyzed: G = galena, KD = K feldspar from disseminated deposit, KV = K feldspar from vein
[2] PC = Precambrian, T = Tertiary
[3] C = center of complex, NM = near margin of complex, OC = outside complex, SC = southcentral part of complex

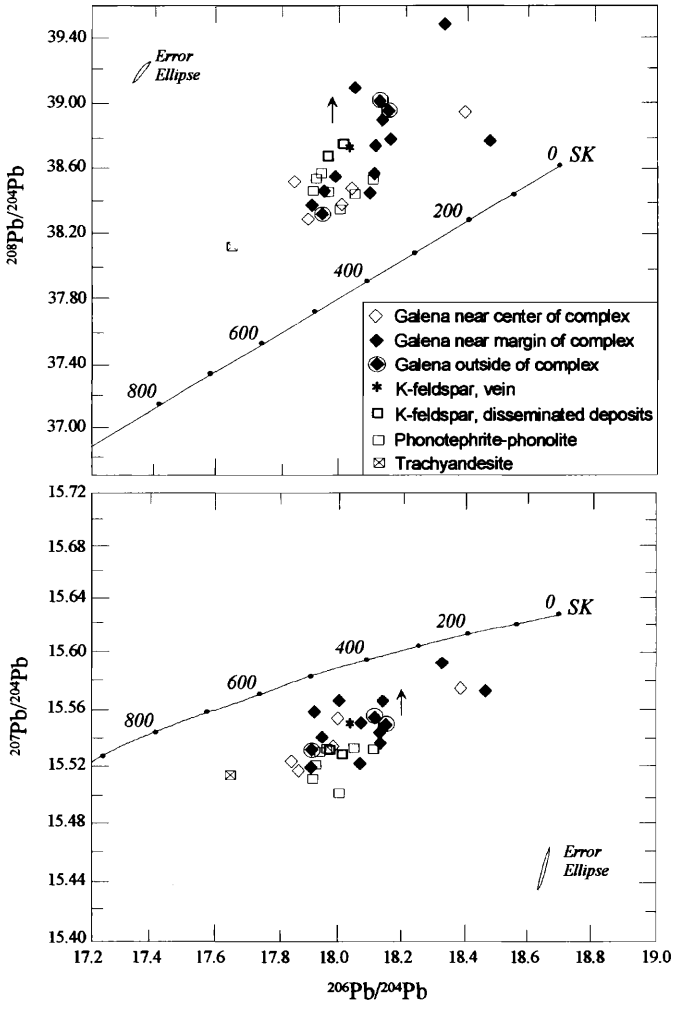

FIG. 15. $^{207}Pb/^{204}Pb$-$^{206}Pb/^{204}Pb$ and $^{208}Pb/^{204}Pb$-$^{206}Pb/^{204}Pb$ plots of Cripple Creek galenas and K feldspar from veins. The lead isotope compositions of the alkaline rocks are shown for comparison. SK = Stacey-Kramers growth curve (Stacey and Kramers, 1975). Small arrows show trends toward relatively more radiogenic $^{207}Pb/^{204}Pb$ and $^{208}Pb/^{204}Pb$ ratios for some galenas collected near the margin or outside the complex, suggesting these galenas contain a component of Precambrian lead; this is particularly evident in the thorogenic lead isotope ratios.

ore fluids cannot account for the relatively high $^{206}Pb/^{204}Pb$ and $^{207}Pb/^{204}Pb$ ratios of some galenas. It is more likely that leaching of the earliest Proterozoic rocks, equivalent to those of the nearby Idaho Springs Formation (1.8 Ga), resulted in the relatively radiogenic galenas. The degree of leaching or the amount of country-rock contamination can be determined using the equation for simple mixing (Powell, 1984). The Pb content of the early Proterozoic rocks (contaminant) is 7 ppm, and the isotope compositions are 19.72, 15.74, and 44.60 for $^{206}Pb/^{204}Pb$, $^{207}Pb/^{204}Pb$, and $^{208}Pb/^{204}Pb$, respectively (Stein, 1985). It is assumed that the ore fluid that deposited the bulk of the galenas (i.e., uncontaminated fluid) had $^{206}Pb/^{204}Pb$, $^{207}Pb/^{204}Pb$, and $^{208}Pb/^{204}Pb$ isotope ratios of 17.94, 15.52, and 38.40, respectively. These are the average values of galenas that are compositionally similar to the phonolitic rocks. The calculations also require knowledge of the concentration of Pb in the ore fluids, which is not known. However, studies by Plumlee (1994) at Creede demonstrate that fluids saturated with respect to galena contained approximately 0.1 ppm Pb. Assuming the ore fluid at Cripple Creek contained 0.1 ppm Pb, only about 1 percent (wt fraction) of contaminant in the fluid mixture would result in a fluid that was highly radiogenic (i.e., $^{208}Pb/^{204}Pb = 40.94$). If the Pb concentration in the ore fluid was 10 ppm, as much as 20 percent of the Pb in the ore fluid would be required from Precambrian rock sources to reach such radiogenic values (Kelley, 1996).

In summary, the close similarity in lead isotope compositions between the phonotephrite-phonolite series of igneous rocks and K feldspar and galenas from veins strongly implies a genetic relationship between mineralized veins and phonolitic rocks. The presence of some relatively radiogenic galenas implies leaching of small amounts of lead from Proterozoic country rocks (Idaho Springs Formation) by the ore fluids. Although it is likely that the Pb (and by inference, perhaps other postgalena ore-related elements) was introduced to the ore fluids directly from the phonolitic magmas, the lead isotope data do not preclude leaching of lead from solid igneous materials by postmagmatic mineralizing fluids. Stable isotope data provide further evidence for the source of the fluids.

Stable isotope data from vein deposits

Previous stable isotope studies at Cripple Creek included district-wide sampling of vein quartz and potassium feldspar for oxygen isotope analyses (Pontius, 1992) and oxygen isotope analyses of vein quartz and wall rocks from the Goldstar (Altman) open-pit area (Beaty et al., 1996). Results from both suggest that the Cripple Creek hydrothermal fluids had a large magmatic water component. The vein $\delta^{18}O_{quartz}$ values range from 13.6 to 18.2 per mil (Pontius, 1992); two samples from the Pharmacist vein system have values as high as 20.7 and 23.7 per mil (Beaty et al., 1996). Vein $\delta^{18}O$ values for K feldspar range from 8.8 to 12.2 per mil (Pontius, 1992).

The $\delta^{18}O$ values for fluids that were in equilibrium with vein quartz or K feldspar are difficult to calculate due to uncertainties in formation temperatures. The temperatures of quartz deposition, in particular, are difficult to assess because quartz was precipitated in the veins throughout the paragenesis, and temperatures could have varied greatly. K feldspar was precipitated only during the early stage of vein formation. The formation temperatures for these early fluids are estimated to be about 250°C (Thompson, 1996). Using the feldspar-water fractionation equation of O'Neil and Taylor (1967), calculated $\delta^{18}O$ fluid compositions in equilibrium with K feldspar at 250°C range from 3.3 to 6.7 per mil.

Vein quartz and whole-rock samples of altered phonolite collected along traverses perpendicular to the axis of the Pharmacist vein system in the Goldstar open pit yielded isotopically heavy oxygen values (Beaty et al., 1996). Vug quartz from the Pharmacist vein had a $\delta^{18}O$ value of 23.7 per mil, and altered phonolite adjacent to and extending out from the Pharmacist vein was significantly enriched in $\delta^{18}O$ (9.3–14.3‰) compared to unaltered phonolite (8–9‰). The hydrothermal fluids responsible for alteration and mineralization had calculated $\delta^{18}O$ values of about 4 to 7 per mil. Beaty et al. (1996) concluded that the high $\delta^{18}O$ value of vein quartz and the substantial and widespread addition of heavy oxygen to wall rocks adjacent to the vein was most likely due to a largely magmatic hydrothermal fluid.

As part of this study, oxygen and hydrogen isotope analyses

were obtained on minerals from hydrothermal veins from selected localities within the district in order to provide additional information on fluid composition and source. K feldspar from a vein at the Ocean Wave mine has a $\delta^{18}O$ value of 7.9 per mil. Biotite from the same vein has a $\delta^{18}O$ value of 3.4 per mil. Primary fluid inclusions in quartz and fluorite from the Newmarket and Bobtail veins in the Ajax mine (Dwelley, 1984) show that early-stage fluids (quartz-biotite-potassium feldspar-fluorite-dolomite-pyrite) were hot (avg 250°C; Thompson, 1996). Assuming a temperature of 250°C for these veins, and using feldspar- and biotite-water fractionation equations of O'Neil and Taylor (1967) and Kyser (1987), calculated fluid compositions in equilibrium with K feldspar and biotite at the Ocean Wave prospect are 2.4 and 4.2 per mil, respectively.

In summary, the calculated fluid compositions in equilibrium with K feldspar and biotite from the early veins range from 2.4 to 6.7 per mil, which partly overlaps the range for typical magmatic water ($\delta^{18}O$ = 5.5–9.5‰; Taylor, 1979). However, interpreting these data in more detail is unwise, due largely to uncertainties in formation temperatures and the sparsity of samples for which $\delta^{18}O$ data are available. Furthermore, these calculated fluid compositions reflect only the early K feldspar and biotite in the veins and not the later ore-stage fluids.

Hydrogen isotope analyses were obtained on two vein biotites: one from the Ocean Wave, for which oxygen is also available, and one from the northern part of the district at the Mollie Kathleen mine. The δD values are −174 and −196 per mil, respectively. Using a temperature of 250°C, and the experimental H/D fractionation equation for biotite and water (Kyser, 1987), calculated δD fluid compositions are −116 and −138 per mil. However, these calculated values may be erroneous. The hydrogen isotope fractionation equation between biotite and water reported by Kyser (1987) was obtained using experiments in pure H_2O at high temperatures (400°–800°C). Therefore, calculating the composition of fluid in equilibrium with Cripple Creek biotites requires extrapolating the D/H fractionation curves beyond the temperature interval over which the experiments were conducted. However, recent questions about the validity of the published fractionation curves, and problems associated with laboratory experiments in which water is used as the exchange medium, strongly caution against extrapolating fractionation curves beyond temperatures of the calibration (Vennemann and O'Neil, 1996). Recent determinations of hydrogen isotope fractionation factors between biotite and molecular hydrogen at temperatures between 150° and 400°C may, therefore, be more appropriate and may yield more accurate results (Vennemann and O'Neil, 1996). At temperatures of 250°C, the calculated fluid compositions are −74 and −96 per mil. Typical magmatic water has δD values of −50 to −85 per mil (Taylor, 1979). Thus, the δD data, similar to the ^{18}O fluid compositions, hint of a magmatic origin for the high-temperature biotite-bearing veins.

Origin of the Cripple Creek Deposits

It is suggested that three important features were collectively responsible for generating alkaline magmas and associated mineral deposits at Cripple Creek. These fundamental factors include: (1) the timing of magmatism and mineralization in relation to tectonic setting, (2) the location of Cripple Creek and the spatial association of mineral deposits with major regional structures, and (3) the complex magmatic history which evolved with time from phonolite to mafic and ultramafic undersaturated magmas.

Timing of magmatism and mineralization in relation to tectonic setting

The generation of alkaline magmas and associated mineral deposits at Cripple Creek (32.5–28.2 Ma) occurred during the transition between active subduction and formation of calc-alkaline magmas (70–40 Ma) and eruption of bimodal volcanism which accompanied the development of the Rio Grande rift (30–27 Ma). Other alkaline rocks in Colorado, formed during this transition, include some in the Colorado mineral belt and Thirtynine Mile volcanic field, as well as isolated complexes such as Rosita Hills and the Spanish Peaks in central and southern Colorado (Fig. 1). These alkaline rocks are part of a widespread north-south belt of alkaline igneous rocks, some of which host important Au (±Te) deposits (Mutschler et al., 1985; Thieben and Spry, 1995; McLemore, 1996; Spry et al., 1996), that extends from Canada to Mexico. Generally, this belt lies along the eastern edge of the Cordillera and east of relatively more significant volumes of coeval or slightly older calc-alkaline rocks.

Some workers have proposed that Cordilleran alkaline magmas are the result of subduction-related processes, and that the K_2O content at a given SiO_2 content is a function of depth to the Benioff zone (Lipman et al., 1972; Keith, 1978). Although the alkaline rocks at Cripple Creek have geochemical and isotopic signatures that argue against a subduction-related tectonic regime (for instance primitive Sr_i ratios and low La/Nb and Zr/Nb ratios), the timing of magmatism and the spatial association of alkaline rocks with coeval or slightly older calc-alkaline rocks (i.e., in the adjacent Thirtynine Mile and Rosita Hills volcanic fields) suggest that there was some association of magmatism with late- or postsubduction zone activity. Postsubduction or back-arc settings is a feature that has recently been recognized for a number of alkaline-related Au deposits (Richards, 1995). In this setting, the driving force responsible for voluminous arc magmatism is not present or has ceased, and melting which does occur in the mantle is usually small in extent and volume, occurring in response to postsubduction tectonic readjustments (Richards, 1995). The exact mechanism and trigger for mantle melting in such settings are still poorly understood.

Location and the spatial association with major regional structures

Another distinguishing feature, perhaps responsible for the great productivity of Cripple Creek, is location. It is the only important metalliferous deposit in Colorado that clearly lies outside of the Colorado mineral belt (Fig. 1; Tweto and Sims, 1963; Tweto, 1968; Romberger, 1980). Other gold-telluride deposits such as the Boulder County deposits in north-central Colorado (Kelly and Goddard, 1969) or those in the La Plata district in southwest Colorado (Eckel, 1949) are within the belt, as are the major porphyry Mo deposits at Climax and Henderson, which are similar in age to Cripple Creek. The intersection of north-south or northwest-trending faults with earlier northeast-trending Laramide (Colorado mineral belt)

structures within the belt is considered to have been a key factor in localizing these deposits (Bookstrom, 1981). Although Cripple Creek lies outside of the mineral belt, it is also associated with major regional structures that provided channelways for focused and prolonged magmatic activity. A major northeast-trending shear zone, formed initially during the Precambrian (Tweto and Sims, 1963; Warner, 1978), lies on the southwest side of the mineral belt and passes through the Quartz Creek area in Gunnison County (Fig. 1) with its dense swarm of crosscutting, northeast-trending pegmatites (Tweto and Sims, 1963). This zone, if projected to the northeast, would pass close to or through Cripple Creek. Direct evidence in the immediate vicinity of Cripple Creek of faults formed during the Proterozoic is a series of northeast-trending faults and shear zones about 5 to 10 km south and southeast of Cripple Creek (i.e., Wilson Creek fault and splays north of Nipple Mountain and east of Brind Mountain; Wobus et al., 1976). These faults are cut by northwest-trending faults formed during the Laramide orogeny or later Rio Grande rift event.

Prolonged and repeated magmatic activity is evident in the vicinity of Cripple Creek. At Cripple Creek, Proterozoic basement (1.8 Ga) was intruded by three separate igneous events at 1.7, 1.4, and 1.0 Ga. During the Laramide orogeny and development of the Rio Grande rift, the northeast-trending faults were reactivated and northwest-trending faults were developed. The Cripple Creek volcanic complex is situated at the junction of the four Proterozoic units and at the intersection of northeast- and northwest-trending faults. Clearly, the region around Cripple Creek was a zone of weakness with structures through which magmas of a wide range in composition were intruded periodically over a long period of time.

Complex magmatic history and evolution of hydrothermal fluids

The last fundamental feature important in the formation of the Cripple Creek deposits was the near-surface emplacement of volatile-rich, alkaline magmas. Although the gold itself cannot be isotopically traced, it is thought that the bulk of the precious metal content was of magmatic origin, introduced into the ore-forming system by magmatic hydrothermal fluids. Direct and indirect supporting evidence of a magmatic origin for the gold deposits at Cripple Creek includes: (1) close spatial association of the deposits with igneous rocks, (2) close temporal association between igneous rocks and associated mineralization and alteration (Table 6), (3) little geochemical or mineralogical zoning over the more than 1,000-m vertical extent of the vein systems, (4) similar lead isotope compositions of galenas from veins and feldspar from igneous rocks (Tables 4 and 7), (5) relatively hot (avg 250°C), hypersaline fluid inclusions reported in quartz from early stages of vein formation (Thompson, 1996), (6) oxygen and hydrogen isotope data for quartz, biotite, and K feldspar from early veins, and (7) similarity of Cripple Creek to other deposits where a magmatic hydrothermal origin is favored, such as the Emperor (Ahmad et al., 1987; Kwak, 1990) and Porgera deposits (Richards and Kerrich, 1993), and those in Montana (Thieben and Spry, 1995; Spry et al., 1996) and New Mexico (McLemore, 1996).

McLemore (1996) suggested that a complex, episodic magmatic history was a key factor for generating the relatively more productive alkalic-related gold deposits in New Mexico. Evidence from Cripple Creek also suggests that the source and evolution of the magmas, and the emplacement history from relatively felsic magmas to successively more mafic magmas with time, may have been important in the evolution of magmatic hydrothermal fluids and the subsequent formation of precious metal deposits. The $^{40}Ar/^{39}Ar$ ages, together with trace element and isotopic data, suggest that postsubduction melting of the mantle produced an alkali- and volatile-rich mafic magma which rose to the base of the lower crust and ponded beneath or was injected within the lower crust where it assimilated lower crust and differentiated by fractional crystallization. The low-viscosity, low-density felsic phonolitic magmas from the top of the chamber ascended first (32.5–30.9 Ma) to shallow levels in the crust. As indicated by oxygen and lead isotope data, upper crustal contamination of the igneous rocks was minor, suggesting that the magmas ascended relatively rapidly. Some of these volatile-rich phonolitic magmas may have encountered water in fractured granite or Tallahassee Creek Conglomerate that resulted in phreatomagmatic eruptions that created initially small breccias and diatremes. Reactivation of major northwest- and northeast-trending faults with time provided structures or magma conduits, and mafic magmas from greater depths were tapped.

Hydrothermal fluids may have evolved from the Cripple Creek magmas in a manner analogous to that described by Burnham (1979) for porphyry systems. During and/or after emplacement of the felsic phonolitic magmas, differentiation proceeded and H_2O (and CO_2, Cl, F, and SO_2) may have been concentrated in the upper parts of the magma body. Breaching of this H_2O-rich carapace by fractures resulted in formation of breccia dikes and pipes above and outward from the magma body. Seepage and diffusive loss of H_2O and heat resulted in precipitation of biotite, K feldspar, fluorite, dolomite, and pyrite in fractures and veinlets; precipitation of K feldspar and pyrite at shallower levels (<300 m) resulted in broad permeable disseminated zones. Mafic phonolite and lamprophyre dikes were intruded after the relatively more felsic rocks, although the exact timing of this event is ambiguous since only a single whole-rock maximum age of 28.7 Ma is indicated. The hydrothermal system continued with precipitation of K feldspar and other gangue minerals followed by native Au and Au-Te minerals. This suggests that with continued evolution of the hydrothermal fluids, many elements (particularly Au and Te) became increasingly concentrated, and/or there was continued influx of Au and Te to the system.

Summary and Conclusions

A list of events, given in approximate geochronological order, that were important in the formation of mineral deposits at Cripple Creek is given as follows:

1. Proterozoic basement (1.8 Ga) was intruded by three separate igneous events at 1.7, 1.4, and 1.0 Ga, and major northeast-trending shear zones and faults were formed.
2. A long period of sedimentation in the early Paleozoic was followed by orogenic uplift and erosion during the late Paleozoic (about 280–320 Ma) which resulted in formation of northwest-trending basins and mountains of the ancestral Rocky Mountains.

3. East-northeast-directed regional compression related to the Late Cretaceous to Tertiary (70–40 Ma) Laramide orogeny formed northwest-trending uplifts and flanking basins. Igneous activity related to the Laramide orogeny included emplacement of alkaline to calc-alkaline rocks that were largely restricted to the Colorado mineral belt.

4. A temporary flattening of the subducting slab to such a low angle resulted in a decrease of igneous activity from about 55 to 40 Ma. Degradation of the mountainous terrane occurred to produce a widespread erosion surface. Between 40 to 35 Ma, there was a renewal of volcanism in Colorado that is believed to be due to a collapsing slab (decreased rate of subduction). This renewal resulted eventually in formation of the San Juan and Thirtynine Mile volcanic fields.

5. The regional change from compressional to extensional tectonics and initial development of the Rio Grande rift began at about 32 to 27 Ma in southern Colorado. Reactivation and development of northwest-trending faults accompanied extension. Initial deposition of volcanic tuffs and volcaniclastic sediments which comprise portions of the Cripple Creek breccia may have formed as early as about 35 Ma.

6. Postsubduction melting of asthenosphere and subcontinental lithospheric mantle generated alkaline, volatile-rich magmas that assimilated and mixed with lower crust and differentiated by fractional crystallization during and/or after ascent.

7. Rapid ascent along crustal fractures and emplacement of the relatively more felsic magmas (32.5–30.9 Ma) at shallow crustal levels was followed by emplacement of mafic and ultramafic alkaline rocks. Field relationships and constraints from $^{40}Ar/^{39}Ar$ ages suggest there may have been more than one episode of mafic-ultramafic igneous activity: one that occurred during the waning stages or shortly after phonolite emplacement and at least one after about 28.7 Ma, as indicated by a single whole-rock age for the Isabella dike (which yielded a maximum age of 28.7 Ma).

8. Gold was deposited after emplacement of mafic and ultramafic rocks, as suggested by field relationships. During the waning stages of fractional crystallization of the phonolitic rocks, K-, S-, and F-rich magmatic-dominant hydrothermal fluids evolved and deposited biotite, K feldspar, dolomite, fluorite, and pyrite followed by gold and gold-telluride minerals in veins throughout a large vertical extent and as disseminated minerals in permeable zones at relatively shallower levels. Available isotopic ages suggest that this began at about 31 to 30 Ma and continued, perhaps intermittently, for at least 2 m.y.

Acknowledgments

This paper represents part of a Ph.D. dissertation completed at the Colorado School of Mines in Golden, Colorado. The authors would like to thank Jeff Griffen and Andy Bordiuk (Texas Gulf) who provided initial access to the property for sample collection. The Pikes Peak Mining Company is thanked for continued field support and access to the Cresson mine. In particular, we thank Tim Harris, Gordon Seibel, and Henry Unger. The senior author is grateful to Scott Birmingham, Craig Simmons, Ian Ridley, Richard Wendlandt, Bill Silberman, and David Kelley for stimulating discussions and provision of relevant information. Dave Allerton, Steve Harlan, and Ross Yeoman (U.S. Geological Survey) are acknowledged for their help with mineral separations, X-ray diffraction analyses, and $^{40}Ar/^{39}Ar$ analyses. Carol Gent provided hydrogen isotope analyses, and whole-rock and trace element chemistry was provided by chemists at the U.S. Geolgical Survey, including Paul Briggs, Al Meier, Rich O'Leary, Jerry Motooka, and Dave Siems. Various versions of this manuscript benefited significantly from reviews by David Kelley (BHP Minerals), Steve Ludington and Rich Goldfarb (U.S. Geological Survey), and two *Economic Geology* reviewers.

March 11, August 12, 1998

REFERENCES

Ahmad, M., Solomon, M., and Walshe, J.L., 1987, Mineralogical and geochemical studies of the Emperor gold telluride deposit, Fiji: Economic Geology, v. 82, p. 345–370.

Alexander, E.C., Michelson, G.M., and Lanphere, M.A., 1978, MMhb-1: A new $^{40}Ar/^{39}Ar$ dating standard: U.S. Geological Survey Open-File Report OF-78-701, p. 6–8.

Anderson, A.T., Clayton, R.N., and Mayeda, T.K., 1971, Oxygen isotope thermometry of mafic igneous rocks: Journal of Geology, v. 79, p. 715–729.

Beaty, D.W., Kelley, K.D., Silberman, M.L., and Thompson, T.B., 1996, Oxygen isotope geochemistry of a portion of the Cripple Creek hydrothermal system: Society of Economic Geologists Guidebook Series, v. 26, p. 55–64.

Birmingham, S.D., 1987, The Cripple Creek volcanic field, central Colorado: Unpub lished M.S. thesis, Austin, University of Texas, 295 p.

Bookstrom, A.A., 1981, Tectonic setting and generation of Rocky Mountain porphyry molybdenum deposits: Arizona Geological Society Digest, v. 14, p. 215–226.

Burnett, W.J., 1995, Fluid chemistry and hydrothermal alteration of the Cresson disseminated gold deposit, Cripple Creek, Colorado: Unpublished M.S. thesis, Fort Collins, Colorado State University, 168 p.

Burnham, C.W., 1979, Magmas and hydrothermal fluids, *in* Barnes, H.L., ed., Geochemis try of hydrothermal ore deposits: New York, Wiley and Sons, p. 71–136.

Carmichael, I.S.E., and Ghiorso, M.S., 1986, Oxidation-reduction relations in basic magma: A case for homogenous equilibria: Earth and Planetary Science Letters, v. 78, p. 200–210.

Catanzaro, E.J., Murphy, T.J., Shields, W.R., and Garner, E.L., 1968, Absolute isotopic abundance ratios of common, equal-atom, and radiogenic lead isotope standards: Journal of Research of the National Bureau of Standards, A. Physics and Chemistry, v. 72A, p. 261–267.

Chapin, C.E., 1979, Evolution of the Rio Grande rift—a summary, Rio Grande rift, *in* Riecker, R.E., ed., Tectonics and magmatism: Washington, D.C., American Geophysical Union, p. 1–5.

Chapin, C.E., and Seager, W.R., 1975, Evolution of the Rio Grande rift in the Socorro and Las Cruces areas: New Mexico Geological Society Guidebook, v. 26, p. 297–321.

Christiansen, R.L., Yeats, R.S., Graham, S.A., Niem, W.A., Niem, A.R., and Snavely, P.D. Jr., 1992, The post-Laramide geology of the U.S. Cordilleran region: Geological Society of America, Geology of North America, v. G3, p. 261–406.

Coney, P.J., 1972, Cordilleran tectonics and North American plate motion: American Journal of Science, v. 272, p. 603–628.

Crock, J.G., Lichte, F.E., and Briggs, P.H., 1983, Determination of elements in National Bureau of Standards geological reference materials SRM 278 obsidian and SRM 688 basalt by inductively coupled argon plasma-atomic emission spectroscopy: Geostandards Newsletter, v. 7, no. 2, p. 335–340.

Cross, W., and Penrose, R.A.F., Jr., 1895, Geology and mining industries of the Cripple Creek district, Colorado: U.S. Geological Survey Sixteenth Annual Report, p. 1–207.

Cunningham, C.G., Naeser, C.W., Marvin, R.F., Luedke, R.G., and Wallace, A.R., 1994, Ages of selected intrusive rocks and associated ore deposits in the Colorado mineral belt: U.S. Geological Survey Bulletin 2109, 31 p

Dalrymple, G.B., and Lanphere, M.A., 1969, Potassium-argon dating: San Francisco, W.H. Freeman Co., 251 p.

Dalrymple, G.B., Alexander, E.C., Lanphere, M.A., and Kraker, G.P., 1981, Irradiation of samples for $^{40}Ar/^{39}Ar$ age dating using the U.S. Geological

Survey TRIGA reactor: U.S. Geological Survey Professional Paper 1176, 56 p.
Doe, B.R., 1970, Lead isotopes: New York, Springer-Verlag, 137 p.
Doe, B.R., and Zartman, R.E., 1979, Plumbotectonics, the Phanerozoic, *in* Barnes, H.L., ed., Geochemistry of hydrothermal ore deposits: New York, Wiley and Sons, p. 22–70.
Dwelley, P.C., 1984, Geology, mineralization, and fluid inclusion analysis of the Ajax vein system, Cripple Creek mining district, Colorado: Unpublished M.S. thesis, Fort Collins, Colorado State University, 167 p.
Eckel, E.B., 1949, Geology and ore deposits of the La Plata district, Colorado: U.S. Geological Survey Professional Paper 219, 179 p.
Epis, R.C., and Chapin, C.E., 1975, Geomorphic and tectonic implications of the post-Laramide, late Eocene erosion surface in the southern Rocky Mountains: Geological Society of America Memoir 144, p. 45–74.
Eriksson, C.L., 1987, Petrology of the alkalic hypabyssal and volcanic rocks at Cripple Creek, Colorado: Unpublished M.S. thesis, Golden, Colorado School of Mines, 114 p.
Evanoff, E., and Chapin, C.E., 1994, Composite nature of the "Late Eocene surface" of the Front Range and adjacent regions, Colorado and Wyoming [abs]: Geological Society of America Abstracts with Programs, v. 26, no. 6, p.12.
Fleck, R.J., Sutter, J.F., and Elliot, D.H., 1977, Interpretation of discordant $^{40}Ar/^{39}Ar$ age-spectra of Mesozoic tholeiites from Antarctica: Geochimica et Cosmochimica Acta, v. 41, p. 15–32.
Geissman, J.W., Snee, L.W., Graaskamp, G.W., Carten, R.B., and Geraghty, E.P., 1992, Deformation and age of the Red Mountain intrusive system (Urad-Henderson molybdenum deposits), Colorado—evidence from paleomagnetic and $^{40}Ar/^{39}Ar$ data: Geological Society of America Bulletin, v. 104, p. 1031–1047.
Godfrey, J.D., 1962, The deuterium content of hydrous minerals from the east-central Sierra Nevada and Yosemite National Park: Geochimica et Cosmochimica Acta, v. 26, p. 1215–1245.
Gott, G. B., McCarthy, J.H., Van Sickle, G.H., and McHugh, J.B., 1969, Distribution of gold and other metals in the Cripple Creek district, Colorado: U.S. Geological Survey Professional Paper 625-A, p. A1–A17.
Harris, T.D., Seibel, G.E., and Pan, G.C., 1993, Information synthesis for the exploration of the Cripple Creek district, Colorado [abs.]: Society of Economic Geology Conference on Integrated Methods in Exploration and Discovery, Denver, Colorado, April 17-20, 1995, Conference Program and Extended Abstracts, p. 49–51.
Hedge, C.E., 1970, Whole-rock Rb-Sr age of the Pikes Peak batholith, Colorado: U.S. Geological Survey Professional Paper 700-B, p. B86–B89.
Hermance, J.F., 1982, Magnetotelluric and geomagnetic deep-sounding studies in rifts and adjacent areas: Constraints on physical processes in the crust and upper mantle, *in* Palmason, G., ed., Continental and oceanic rifts: Washington, DC, American Geophysical Union,p. 169–192.
Hubert, A.E., and Chao, T.T., 1985, Determination of gold, indium, tellurium, and thallium in the same sample digestion of geological materials by atomic-absorption spectroscopy and two-step solvent extraction: Talanta, v. 32, p. 568–570.
Hutchinson, R.M., and Hedge, C.E., 1968, Depth-zone emplacement and geochronology of Precambrian plutons, central Colorado Front Range: Geological Society of America Special Paper 115, p. 424–425.
Irvine, T.N., and Baragar, W.R.A., 1971, A guide to the chemical classification of the common volcanic rocks: Canadian Journal of Earth Sciences, v. 8, p. 523–548.
Jensen, E.P., and Barton, M.D., 1997, Types of potassium silicate alteration and related base metal mineralization in the Cripple Creek district, Colorado [abs]: Geological Society of America Abstracts with Programs, v. 29, no. 6, p. A-207.
Keith, S.B., 1978, Paleosubduction geometries inferred from Cretaceous and Tertiary magmatic patterns in southwestern North America: Geology, v. 6, p. 516–521.
Kelley, K.D., 1996, Origin and timing of magmatism and mineralization in the Cripple Creek district, Colorado: Unpublished Ph.D dissertation, Golden, Colorado School of Mines, 259 p.
Kelly, W.C., and Goddard, E.N., 1969, Telluride ores of Boulder County, Colorado: Geological Society of America Memoir 109, 237 p.
Kleinkopf, M.D., Peterson, D.L., and Gott, G.B., 1970, Geophysical studies of the Cripple Creek mining district, Colorado: Geophysics, v. 35, p. 490–500.
Koschmann, A.H., 1949, Structural control of the gold deposits of the Cripple Creek district, Colorado: U.S. Geological Survey Bulletin 955-B, 60 p.
Koschmann, A.H., and Loughlin, G.F., 1965, Mine maps of the Cripple Creek district, Colorado: U.S. Geological Survey Open-File Report 65-90.
Kwak, T.A.P., 1990, Geochemical and temperature controls on ore mineralization at the Emperor gold mine, Vatukoula, Fiji: Journal of Geochemical Exploration, v. 36, p. 297–337.
Kyser, T.K., 1987, Equilibrium fractionation factors for stable isotopes: Mineralogical Association of Canada Short Course, v. 13, p. 1–84.
Kyser, T.K., O'Neil, J.J., and Carmichael, I.S.E., 1982, Genetic relations among basic lavas and ultramafic nodules: Evidence from oxygen isotope compositions: Contributions to Mineralogy and Petrology, v. 81, p. 88–102.
Lane, C.A., 1976, Geology, mineralogy and fluid inclusion geothermometry of the El Paso mine, Cripple Creek, Colorado: Unpublished M.S. thesis, University of Missouri-Rolla, 103 p.
Lanphere, M.A., and Dalrymple, G.B., 1976, Identification of excess ^{40}Ar by the $^{40}Ar/^{39}Ar$ age spectrum technique: Earth and Planetary Science Letters, v. 32, p. 141–148.
Le Bas, M.J., Le Maitre, R.W., Streckeisen, A., and Zanettun, B., 1986, A chemical classification of volcanic rocks based on the total alkali-silica diagram: Journal of Petrology, v. 27, p. 745–750.
Lindgren, W., and Ransome, F.L., 1906, Geology and gold deposits of the Cripple Creek district, Colorado: U.S. Geological Survey Professional Paper 54, 516 p.
Lipman, P.W., 1981, Volcano-tectonic setting of Tertiary ore deposits, southern Rocky Mountains: Arizona Geological Society Digest, v. 14, p. 199–213.
Lipman, P.W., Prostka, H.J., and Christiansen, R.L., 1972, Cenozoic volcanism and plate-tectonic evolution of the western United States: Part 1. Early and middle Cenozoic: Royal Society of London Philosophical Transactions, v. 271, p. 217–248.
Lipman, P.W., Doe, B.R., Hedge, C.E., and Steven, T.A., 1978, Petrologic evolution of the San Juan volcanic field, southwestern Colorado: Pb and Sr isotope evidence: Geological Society of America Bulletin, v. 89, p. 59–82.
Livo, K.E., 1994, Use of remote sensing to characterize hydrothermal alteration of the Cripple Creek area, Colorado: Unpublished M.S. thesis, Golden, Colorado School of Mines, 135 p.
Loughlin, G.F., and Koschmann, A.H., 1935, Geology and ore deposits of the Cripple Creek district, Colorado: Colorado Scientific Society Proceedings, v. 13, no. 6, p. 217–435.
McDonough, W.F., McCulloch, M.T., and Sun, S.S., 1985, Isotopic and geochemical systematics in Tertiary-Recent basalts from southeastern Australia and implications for the evolution of the sub-continental lithosphere: Geochimica et Cosmochimica Acta, v. 49, p. 2051–2067.
McDowell, F.W., 1971, K-Ar ages of igneous rocks from the western United States: Isochron West, no. 2, 16 p.
McLemore, V.T., 1996, Great Plains Margin (alkaline-related) gold deposits in New Mexico: Geological Society of Nevada Geology and Ore Deposits of the American Cordillera Symposium, Reno-Sparks, Nevada, April 10-13, 1995, Proceedings, v. 3, p. 1341–1354.
Meier, A.L., Grimes, D.J., and Ficklin, W.H., 1994, Inductively coupled plasma mass spectrometry—a powerful analytical tool for mineral resource and environmental studies: U.S. Geological Survey Circular 1103-A, p. 67–68.
Mertzman, S.A., Wobus, R.A., Kroeger, G., 1994, The Thirtynine Mile volcanic field of central Colorado: The Guffey volcanic center and surrounding areas [abs]: Geological Society of America Abstracts with Programs, v. 26, no. 6, p. 54.
Mutschler, F.E., and Mooney, T.C., 1995, Precious metal deposits related to alkaline igneous rocks—provisional classification, grade-tonnage data, and exploration frontiers: Geological Association of Canada Special Paper 40, p. 479-520.
Mutschler, F.E., Griffin, M.E., Stevens, D.S., and Shannon, S.S. Jr., 1985, Precious metal deposits related to alkaline rocks in the North American Cordillera—an interpretive review: Geological Society of South Africa Transactions, v. 88, p. 355–377.
Nelson, S.E., 1989, Geology, alteration, and mineral deposits of the Cresson diatreme, Cripple Creek district, Colorado: Unpublished M.S. thesis, Fort Collins, Colorado State University, 147 p.
O'Leary, R.M., and Meier, A.L., 1986, Analytical methods used in geochemical exploration, 1984: U.S. Geological Survey Circular 948, p. 21–23.
O'Neil, J.R., and Taylor, H.P. Jr., 1967, The oxygen isotope and cation exchange chemistry of feldspars: American Mineralogist, v. 52, p. 1414–1437.

Plumlee, G.S., 1994, Fluid chemistry evolution and mineral deposition in the main-stage Creede epithermal system: ECONOMIC GEOLOGY, v. 89, p. 1860–1882.
Pontius, J.A., 1992, Gold mineralization within the Cripple Creek diatreme/volcanic complex, Cripple Creek mining district, Colorado, USA: Minexpo 92, Las Vegas, Nevada, October 18-22, Proceedings, 12 p.
——1996, Gold deposits of the Cripple Creek mining district, Colorado, USA: Society of Economic Geologists Guidebook Series, v. 26, p. 29–37.
Powell, R., 1984, Inversion of the assimilation and fractional crystallization (AFC) equations: Characterization of contaminants from isotope and trace element relationships in volcanic suites: Geological Society of London Journal, v. 141, p. 447–452.
Reed, J.C., Jr., Bickford, M.E., Premo, W.R., Aleinikoff, J.N., and Pallister, J.S., 1987, Evolution of the Early Proterozoic Colorado province: Geology, v. 15, p. 861–865.
Richards, J.P., 1995, Alkalic-type epithermal deposits—a review: Mineralogical Association of Canada Short Course Series, v. 23, p. 367–400.
Richards, J.P., and Kerrich, R., 1993, The Porgera gold mine, Papua New Guinea: Magmatic hydrothermal to epithermal evolution of an alkalic-type precious metal deposit: ECONOMIC GEOLOGY, v. 88, p. 1017–1052.
Roddick, J.C., 1983, High precision intercalibration of Ar-Ar standards: Geochimica et Cosmochimica Acta, v. 47, p. 887–898.
Romberger, S.B., 1980, Metallic mineral resources of Colorado, *in* Kent, H.C., and Porter, K.W., eds., Colorado geology: Denver, Rocky Mountain Association of Geologists, p. 225–236.
Saunders, J.A., 1986, Petrology, mineralogy, and geochemistry of representative gold telluride ores from Colorado: Unpublished Ph.D dissertation, Golden, Colorado School of Mines, 171 p.
Seibel, G.E., 1991, Geology of the Victor mine, Cripple Creek mining district, Colorado: Unpublished M.S. thesis, Fort Collins, Colorado State University, 133 p.
Smith, A.E., Raines, E., and Feitz, L., 1985, The Cresson Vug, Cripple Creek: Mineralogical Record, v. 16, p. 231–238.
Snee, L.W., Sutter, J.F., and Kelly, W.C., 1988, Thermochronology of economic mineral deposits: Dating the stages of mineralization at Panasqueira, Portugal, by high-precision $^{40}Ar/^{39}Ar$ age spectrum techniques on muscovite: ECONOMIC GEOLOGY, v. 83, p. 335–354.
Spry, P.G., Paredes, M.M., Foster, Fess, Truckle, J.S., and Chadwick, T.H., 1996, Evidence for a genetic link between gold-silver telluride and porphyry molybdenum mineralization at the Golden Sunlight deposit, Whitehall, Montana: Fluid inclusion and stable isotope studies: ECONOMIC GEOLOGY, v. 91, p. 507–526.
Stacey, J.S., and Kramers, J.D., 1975, Approximation of terrestrial lead isotope evolution by a two-stage model: Earth and Planetary Science Letters, v. 26, p. 207–221.
Steiger, R.H., and Jäger, E., 1977, Subcommission on geochronology: Convention on the use of decay constants in geo- and cosmo-chronology: Earth and Planetary Science Letters, v. 36, p. 359–362.
Stein, H.J., 1985, A lead, strontium, and sulfur isotope study of Laramide-Tertiary intrusions and mineralization in the Colorado mineral belt with emphasis on Climax-type porphyry molybdenum systems plus a summary of other newly acquired isotopic and rare earth element data: Unpublished Ph.D. dissertation, Chapel Hill, University of North Carolina, 493 p.
Taggart, Joseph E., Jr., Lindsey, J.R., Scott, B.A., Vivit, D.V., Bartel, A.J., and Stewart, K.C., 1987, Analysis of geological materials by wavelength-dispersive X-ray fluorescence spectrometry: U.S. Geological Survey Professional Paper 1770, p. E1-E19.
Taranik, D.L., 1990, Remote detection and mapping of supergene iron oxides in the Cripple Creek district: Unpublished M.S. thesis, Boulder, University of Colorado, 103 p.
Taylor, H.P. Jr., 1968, The oxygen isotope geochemistry of igneous rocks: Contribu tions to Mineralogy and Petrology, v. 19, p. 1–71.
——1979, Oxygen and hydrogen isotope relationships in hydrothermal mineral deposits, *in* Barnes, H.L., ed., Geochemistry of hydrothermal ore deposits, 2nd ed.: New York, John Wiley and Sons, p. 236–277.
Taylor, H.P., Jr., and Epstein, S., 1962a, Relationships between $^{18}O/^{16}O$ ratios in coexisting minerals of igneous and metamorphic rocks: Part 1. Principles and experimental results: Geological Society of America Bulletin, v. 73, p. 461–480.
——1962b, Relationships between $^{18}O/^{16}O$ ratios in coexisting minerals of igneous and metamorphic rocks: Part 2. Applications to petrologic problems: Geological Society of America Bulletin, v. 73, p. 675–694.
Taylor, H.P., Jr., and Sheppard, S.M.F., 1986, Igenous rocks: I. Processes of isotopic fractionation and isotope systematics: Reviews in Mineralogy, v. 16, p. 227–271.
Taylor, H.P., Jr., Frechen, J., and Degens, E.T., 1967, Oxygen and carbon isotope studies of carbonatites from the Laacher See district, West Germany and the Alnö district, Sweden: Geochimica et Cosmochimica Acta, v. 31, p. 407–430.
Taylor, S.R., and McLennan, S.M., 1985, The continental crust: Its composition and evolution: Oxford, Blackwell Scientific Publications, 312 p.
Thieben, S.E., and Spry, P.G., 1995, The geology and geochemistry of Cretaceous-Tertiary alkaline igneous rock-related gold-silver telluride deposits of Montana, USA, *in* Pasava, J., Kříbek, B., and Žák, K., eds., Mineral deposits: Rotterdam, Balkema, p. 199–202.
Thompson, T.B., 1989, The Cripple Creek district: International Geological Congress, 28th, Washington, D.C, July 1-8, 1989, Field Trip Guidebook T129, p. 62–73.
——1992, Mineral deposits of the Cripple Creek district, Colorado: Mining Engineering, v. 44, p. 135–138.
——1996, Fluid evolution of the Cripple Creek hydrothermal system, Colorado: Society of Economic Geologists Guidebook Series, v. 26, p. 45–54.
Thompson, T.B., Trippel, A.D., and Dwelley, P.C., 1985, Mineralized veins and breccias of the Cripple Creek district, Colorado: ECONOMIC GEOLOGY, v. 80, p. 1669–1688.
Trippel, A.D., 1985, Hydrothermal mineralization and alteration at the Globe Hill deposit, Cripple Creek district, Colorado: Unpublished M.S. thesis, Fort Collins, Colorado State University, 93 p.
Tweto, O., 1968, Geologic setting and interrelationships of mineral deposits in the mountain province of Colorado and south central Wyoming, *in* Ridge, J.D., ed., Ore deposits in the United States 1933-1967 (Graton-Sales volume): New York, American Institute Mining, Metallurgical, and Petroleum Engineers, v. 1, p. 551–588.
——1980, Tectonic history of Colorado, *in* Kent, H.C., and Porter, K.W., eds., Colorado geology: Denver, Rocky Mountain Association of Geologists, p. 5–9.
Tweto, O., and Sims, P.C., 1963, Precambrian ancestry of the Colorado mineral belt: Geological Society of America Bulletin, v. 74, p. 991–1014.
Vennemann, R.W., and O'Neil, J.R., 1996, Hydrogen isotope exchange reactions between hydrous minerals and molecular hydrogen: I. A new approach for the determination of hydrogen isotope fractionation at moderate temperatures: Geochimica et Cosmochimica Acta, v. 60, p. 2437–2451.
Wallace, A.R., 1990, Regional geologic and tectonic setting of the central Colorado mineral belt: Paleozoic stratigraphy, tectonism, thermal history, and basin evolution of central Colorado: ECONOMIC GEOLOGY MONOGRAPH 7, p. 19–28.
Wallace, S.R., 1995, Presidential address—the Climax-type molybdenite deposits: What they are, where they are, and why they are: ECONOMIC GEOLOGY, v. 90, p. 1359–1380.
Warner, L., 1978, The Colorado lineament: A middle Precambrian wrench fault system: Geological Society of America Bulletin, v. 89, p. 161–171.
Weaver, S.D., Sceal, J.S.C., and Gibson, I.C., 1972, Trace element data relevant to the origin of trachytic and pantelleritic lavas in the east African rift system: Contributions to Mineralogy and Petrology, v. 36, p. 181–194.
Wendlandt, E.D., DePaolo, D.J., and Baldridge, W.S., 1991, Nd, Sr, and O isotope constraints on magmatic underplating of the lower crust beneath the Rio Grande rift, NM [abs.]: Geological Society of America Abstracts with Programs, v. 23, no. 5, p. 104.
Wilson, M., 1989, Igneous petrogenesis: London, UK, Chapman and Hall, 466 p.
Wobus, R.A., Epis, R.C., and Scott, G.R., 1976, Reconnaissance geologic map of the Cripple Creek-Pikes Peak area, Teller, Fremont, and El Paso Counties, Colorado: U.S. Geological Survey Miscellaneous Field Studies Map MF-805.
Wood, M.R., 1990, Geology and alteration of the eastern Cripple Creek mining district, Teller County, Colorado: Unpublished M.S. thesis, Fort Collins, Colorado State University, 186 p.
Wörner, G., Harmon, R.S., and Hoefs, J., 1987, Stable isotope relations in an open magma system, Laacher See, Eifel (FRG): Contributions to Mineralogy and Petrology, v. 95, p. 343–349.
York, D., 1969, Least squares fitting of a straight line with correlated errors: Earth and Planetary Science Letters, v. 5, p. 320–324.
Zartman, R.E., and Doe, B.R., 1981, Plumbotectonics—the model: Tectonophysics, v. 75, p. 135–162.
Zartman, R.E., and Haines, S.M., 1988, The plumbotectonic model for Pb isotopic systematics among major terrestrial reservoirs—a case for bidirectional transport: Geochimica et Cosmochimica Acta, v. 52, p. 1327–1339.

APPENDIX

$^{40}Ar/^{39}Ar$ Data for Igneous Rocks and Mineralized Samples from the Cripple Creek District

Temp (°C)	$^{40}Ar_R$	$^{39}Ar_K$	F	$^{39}Ar_K$ (% of total)	$^{40}Ar_{rad}$ (%)	$^{39}Ar/^{37}Ar$	Apparent age ±1σ (Ma)
Sample: 89CC004, sanidine from phonolite, J = 0.007284, sample wt = 54.1 mg							
600	0.18684	0.06585	2.837	1.6	70.2	3.94	36.91 ± .24
700	0.53834	0.21804	2.469	5.2	65.7	5.24	32.16 ± .31
800	2.26982	0.93709	2.422	22.2	93.2	7.57	31.55 ± .07
900	1.76551	0.72192	2.446	17.1	97.7	8.90	31.85 ± .12
1,000	1.43601	0.59342	2.420	14.1	95.1	10.64	31.52 ± .06
1,050	0.67267	0.27375	2.457	6.5	95.8	10.22	32.00 ± .16
1,100	0.88453	0.36308	2.436	8.6	95.6	10.09	31.73 ± .22
1,150	1.53529	0.62895	2.441	14.9	97.0	11.60	31.79 ± .11
1,200	0.88445	0.36201	2.443	8.6	96.1	11.20	31.82 ± .12
1,250	0.14498	0.05936	2.442	1.4	90.0	8.54	31.81 ± 1.15
Total gas age = 31.8 ± 0.1 Ma							
Plateau age = 31.8 ± 0.1 Ma							
Sample: 89CCPH1, sanidine from phonolite, J = 0.007312, sample wt = 64.3 mg							
600	0.40217	0.16332	2.462	3.9	36.2	33.17	32.19 ± .21
700	0.94388	0.38968	2.422	9.3	76.4	36.48	31.67 ± .20
800	1.39668	0.59079	2.364	14.2	89.3	33.20	30.92 ± .10
900	0.86294	0.36351	2.374	8.7	92.0	24.64	31.05 ± .15
1,000	0.96555	0.40987	2.356	9.8	91.4	22.53	30.81 ± .08
1,050	0.94292	0.40098	2.352	9.6	90.9	24.94	30.75 ± .16
1,100	2.09188	0.88419	2.366	21.2	88.8	26.76	30.94 ± .05
1,150	1.78995	0.74397	2.406	17.8	83.3	24.43	31.46 ± .05
1,200	0.36239	0.13950	2.598	3.3	79.0	21.03	33.94 ± .52
1,250	0.12331	0.05395	2.286	1.3	71.0	22.34	29.90 ± .26
1,350	0.07542	0.03417	2.207	0.8	63.8	17.86	28.89 ± 1.35
Total gas age = 31.2 ± 0.1 Ma							
Plateau age = 30.9 ± 0.1 Ma							
Sample: 89CC009, sanidine from phonolite, J = 0.007402, sample wt = 87.8 mg							
600	0.77579	0.10191	7.612	1.3	71.6	19.35	98.89 ± .34
700	1.56269	0.58732	2.661	7.3	81.5	28.83	35.18 ± .05
800	2.65897	1.11092	2.393	13.8	95.9	31.74	31.68 ± .07
850	1.12055	0.47042	2.382	5.8	94.6	31.35	31.53 ± .14
900	0.86768	0.35281	2.459	4.4	92.8	31.78	32.54 ± .12
1,000	2.51865	0.82783	3.042	10.3	91.3	31.15	40.18 ± .06
1,050	3.08117	0.99306	3.103	12.3	89.5	32.21	40.96 ± .06
1,100	6.31573	1.52164	4.151	18.9	91.0	34.99	54.59 ± .11
1,150	6.80496	1.50700	4.516	18.7	93.4	36.54	59.31 ± .09
1,200	1.68203	0.39230	4.288	4.9	93.1	32.24	56.36 ± .16
1,250	0.54068	0.11613	4.656	1.4	91.1	24.26	61.12 ± .15
1,350	0.34834	0.04809	7.243	0.6	92.6	10.46	94.22 ± .50
1,450	0.15683	0.03299	4.754	0.4	77.9	2.33	62.40 ± 1.49
Total gas age = 46.5 ± 0.1 Ma							
No plateau							
Sample: 89CC010S, sanidine from tephriphonolite, J = 0.007541, sample wt = 56.9							
600	0.19201	0.06285	3.055	1.1	32.4	2.43	41.09 ± 1.39
700	1.30033	0.51747	2.513	9.0	84.6	10.30	33.87 ± .22
800	1.46799	0.60799	2.414	10.6	84.0	8.51	32.55 ± .16
900	1.04382	0.43693	2.389	7.6	94.6	5.70	32.21 ± .10
1,000	1.37733	0.57812	2.382	10.1	93.3	8.67	32.12 ± .11
1,050	1.94761	0.80781	2.411	14.1	94.8	16.34	32.50 ± .09
1,100	2.66015	1.10528	2.407	19.3	94.9	19.44	32.45 ± .05
1,150	2.98375	1.24033	2.406	21.7	95.9	21.47	32.43 ± .05
1,200	0.76002	0.31383	2.422	5.5	95.6	9.41	32.65 ± .05
1,250	0.07810	0.03232	2.416	0.6	81.3	2.04	32.58 ± .92
1,350	0.06343	0.02527	2.510	0.4	74.4	1.27	33.82 ± 2.19
Total gas age = 32.7 ± 0.1 Ma							
Plateau age = 32.5 ± 0.1 Ma							

APPENDIX (*Cont.*)

Temp (°C)	$^{40}Ar_R$	$^{39}Ar_K$	F	$^{39}Ar_K$ (% of total)	$^{40}Ar_{rad}$ (%)	$^{39}Ar/^{37}Ar$	Apparent age ±1σ (Ma)
Sample: 530N2, biotite from tephriphonolite dike, J = 0.005322, sample wt = 35.1 mg							
600	0.07922	0.02444	3.241	.9	20.8	1.96	30.85 ± .50
700	0.22667	0.06497	3.489	2.3	40.5	0.72	33.19 ± .15
750	0.36535	0.10601	3.446	3.7	87.2	27.14	32.79 ± .13
800	0.60295	0.17795	3.388	6.3	91.4	73.91	32.24 ± .17
850	0.80717	0.23686	3.408	8.3	92.3	101.37	32.42 ± .16
900	0.98097	0.29060	3.376	10.2	92.6	108.86	32.12 ± .10
950	1.08108	0.31850	3.394	11.2	92.8	118.30	32.30 ± .05
1,000	0.87346	0.25827	3.382	9.1	88.9	43.46	32.18 ± .05
1,050	1.91146	0.56036	3.411	19.7	88.3	6.43	32.46 ± .08
1,300	2.72946	0.80357	3.397	28.3	88.7	10.79	32.32 ± .05
Total gas age = 32.34 ± .08 Ma							
Plateau age = 32.31 ± .09 Ma							
Sample: 89CC005, whole rock of phonotephrite—Isabella dike, J = 0.007481, sample wt = 233.3 mg							
400	0.22015	0.09789	2.249	1.0	23.8	3.66	30.10 ± .49
500	0.34221	0.15883	2.155	1.6	54.4	7.92	28.84 ± .22
600	1.24297	0.55963	2.221	5.6	76.7	9.27	29.73 ± .07
700	2.32460	0.98502	2.360	9.8	78.3	8.22	31.57 ± .05
800	2.77528	1.20464	2.304	12.0	90.6	7.85	30.83 ± .05
900	2.51985	1.09378	2.304	10.9	90.8	6.22	30.83 ± .06
1,000	3.12279	1.41036	2.214	14.0	93.0	4.72	29.64 ± .07
1,100	6.48312	3.02781	2.141	30.1	94.3	4.75	28.67 ± .04
1,200	2.91280	1.31630	2.213	13.1	93.7	0.24	29.62 ± .05
1,300	0.30031	0.13016	2.307	1.3	88.6	0.05	30.87 ± .21
1,400	0.17625	0.08079	2.182	0.8	81.5	0.05	29.20 ± .78
Total gas age = 29.8 ± 0.1 Ma							
Sample: 89CC007, whole rock of trachyandesite, J = 0.007459, sample wt = 266.4 mg							
400	0.04142	0.01696	2.442	0.9	13.5	3.62	32.58 ± 2.82
500	0.02572	0.01074	2.395	0.6	14.2	3.79	31.95 ± 4.22
600	0.08009	0.02919	2.744	1.6	26.5	5.15	36.55 ± .53
700	0.18265	0.06766	2.700	3.7	42.8	5.75	35.97 ± .38
800	0.27163	0.10182	2.668	5.5	61.4	5.23	35.55 ± .42
900	0.41519	0.16379	2.535	8.9	74.0	6.31	33.79 ± .35
1,100	1.06654	0.44415	2.401	24.1	89.6	7.53	32.03 ± .05
1,200	0.97025	0.40312	2.407	21.8	92.0	7.10	32.10 ± .12
1,300	0.50835	0.21342	2.382	11.6	89.4	7.09	31.77 ± .07
1,400	0.93360	0.39576	2.359	21.4	83.0	6.74	31.47 ± .08
Total gas age = 32.5 ± 0.2 Ma							
Sample: 37K122, biotite from vein, J = 0.007604, sample wt = 60.8 mg							
600	0.05580	0.03293	1.695	0.5	14.6	0.73	23.09 ± .17
700	0.74472	0.32242	2.310	4.9	52.1	12.90	31.41 ± .05
750	0.84235	0.37686	2.235	5.7	80.5	258.41	30.40 ± .17
800	1.27942	0.57667	2.219	8.7	89.5	951.48	30.18 ± .10
850	1.80001	0.81871	2.199	12.4	93.2	1900.35	29.91 ± .06
900	1.20173	0.54551	2.203	8.2	92.7	1882.89	29.97 ± .05
950	0.72234	0.32659	2.212	4.9	90.0	993.45	30.09 ± .17
1,000	0.62364	0.28210	2.211	4.3	88.6	594.45	30.07 ± .13
1,050	1.53144	0.69515	2.203	10.5	94.2	1441.22	29.97 ± .05
1,150	4.11042	1.87039	2.198	28.3	94.4	1302.06	29.90 ± .05
1,300	1.68971	0.76505	2.209	11.6	91.2	430.88	30.05 ± .06
Total gas age = 29.9 ± .1 Ma							
Plateau age = 29.9 ± .1 Ma							

APPENDIX (*Cont.*)

Temp (°C)	$^{40}Ar_R$	$^{39}Ar_K$	F	$^{39}Ar_K$ (% of total)	$^{40}Ar_{rad}$ (%)	$^{39}Ar/^{37}Ar$	Apparent age ±1σ (Ma)
Sample: 89CC003, adularia from vein, J = 0.005392, sample wt = 17.8 mg							
500	0.12099	0.02571	4.705	1.1	14.7	58.44	45.20 ± .43
600	0.24006	0.07019	3.420	3.1	58.4	30.26	32.96 ± .05
650	0.11168	0.04489	2.488	2.0	22.2	17.06	24.04 ± .91
700	0.16851	0.05306	3.176	2.4	59.1	549.76	30.63 ± .59
800	0.47705	0.14532	3.283	6.4	68.8	549.56	31.65 ± .05
900	0.67327	0.21135	3.186	9.4	75.5	722.79	30.72 ± .16
1,000	0.81428	0.25118	3.242	11.1	79.3	586.41	31.26 ± .08
1,100	1.16065	0.35871	3.236	15.9	81.7	1045.44	31.20 ± .05
1,350	3.55246	1.09577	3.242	48.6	79.7	1349.18	31.26 ± .05
Total gas age = 31.28 ± .1 Ma							
Plateau age = 31.25 ± .06 Ma							
Sample: CC-2, adularia from vein, J = 0.007905, sample wt = 41.6 mg							
500	0.07860	0.02512	3.129	0.2	16.1	173.66	44.08 ± .38
600	0.64460	0.29443	2.189	2.9	45.4	3452.99	30.95 ± .05
700	1.49542	0.70558	2.119	6.9	60.0	716.00	29.97 ± .05
800	1.58648	0.75513	2.101	7.4	86.6	3451.52	29.71 ± .05
900	1.95671	0.93755	2.087	9.1	90.6	3950.84	29.52 ± .08
1,000	2.40761	1.15215	2.090	11.2	90.1	261.51	29.56 ± .06
1,100	4.69908	2.24815	2.090	21.9	89.2	591.59	29.56 ± .08
1,200	5.50106	2.62011	2.100	25.5	87.3	366.52	29.70 ± .05
1,450	3.20280	1.52777	2.096	14.9	90.2	341.07	29.65 ± .05
Total gas age = 29.72 ± .06 Ma							
Plateau age = 29.61 ± .06 Ma							
Sample: CRESA-4, adularia from breccia with disseminated mineralization, J = 0.00795, sample wt = 76.1 mg							
500	0.07860	0.02512	3.129	0.2	16.1	198.98	50.77 ± .84
600	0.64460	0.29443	2.189	2.9	45.4	890.62	31.02 ± .13
700	1.49542	0.70558	2.119	6.9	60.0	266.70	29.82 ± .05
800	1.58648	0.75513	2.101	7.4	86.6	1366.55	29.79 ± .05
900	1.95671	0.93755	2.087	9.1	90.6	3562.55	29.57 ± .26
1,000	2.40761	1.15215	2.090	11.2	90.1	2945.95	30.05 ± .06
1,100	4.69908	2.24815	2.090	21.9	89.2	1201.61	31.24 ± .07
1,200	5.50106	2.62011	2.100	25.5	87.3	3950.67	32.95 ± .05
1,400	3.20280	1.52777	2.096	14.9	90.2	690.27	33.49 ± .05
Total gas age = 30.93 ± .08 Ma							
Plateau age = 29.76 ± .12 Ma							
Sample: 89CC001A sanidine from altered phonolite, J = 0.00774, sample wt = 95.8 mg							
600	0.67075	0.29354	2.285	1.5	27.3	509.47	31.63 ± .12
700	3.54630	1.66873	2.125	8.6	83.0	1040.32	29.43 ± .05
800	2.63776	1.23604	2.134	6.4	79.1	821.61	29.55 ± .05
850	1.14510	0.54295	2.109	2.8	82.6	1131.36	29.21 ± .08
900	1.04862	0.49983	2.098	2.6	85.5	930.17	29.06 ± .09
950	1.29127	0.61499	2.100	3.2	87.9	1081.77	29.08 ± .05
1,000	1.60077	0.76162	2.102	3.9	90.2	1081.47	29.11 ± .07
1,050	2.66848	1.28148	2.082	6.6	89.7	1068.62	28.84 ± .08
1,100	3.09117	1.48766	2.078	7.7	88.8	1085.81	28.78 ± .05
1,150	4.93639	2.36415	2.088	12.2	86.2	1230.46	28.92 ± .04
1,200	7.76064	3.70547	2.094	19.1	79.4	1674.14	29.01 ± .04
1,250	8.34949	3.95672	2.110	20.4	75.3	2283.71	29.23 ± .05
1,350	1.32886	0.62209	2.136	3.2	71.2	896.38	29.58 ± .08
1,450	0.71530	0.32833	2.179	1.7	66.2	1537.45	30.17 ± .22
Total gas age = 29.2 ± 0.1 Ma							

APPENDIX (*Cont.*)

Temp (°C)	$^{40}Ar_R$	$^{39}Ar_K$	F	$^{39}Ar_K$ (% of total)	$^{40}Ar_{rad}$ (%)	$^{39}Ar/^{37}Ar$	Apparent age $\pm 1\sigma$ (Ma)
Sample: 89CC001B, sanidine from altered phonolite, J = 0.007548, sample wt = 86.0 mg							
600	1.00482	0.44731	2.246	2.6	33.2	593.38	30.33 ± .06
700	2.49869	1.17870	2.120	6.8	68.3	826.13	28.64 ± .05
800	1.64888	0.77603	2.125	4.5	67.1	733.51	28.70 ± .09
900	1.43443	0.68242	2.102	3.9	61.7	774.60	28.40 ± .09
1,000	2.06822	0.98046	2.109	5.7	69.3	1022.21	28.50 ± .05
1,050	2.18763	1.04721	2.089	6.0	77.3	1248.02	28.22 ± .06
1,100	2.50688	1.19194	2.103	6.9	81.5	1411.91	28.41 ± .11
1,150	3.69126	1.75527	2.103	10.1	81.0	1270.87	28.41 ± .05
1,200	8.44147	4.01336	2.103	23.2	75.9	1823.79	28.42 ± .04
1,250	9.97056	4.69571	2.123	27.1	73.5	3196.89	28.68 ± .05
1,350	0.91491	0.42189	2.169	2.4	57.2	1672.10	29.29 ± .16
1,450	0.28131	0.12662	2.222	0.7	36.4	894.48	30.00 ± .35
Total gas age = 28.4 ± 0.1 Ma							